Mathematical model of CISH knockout predicts increased efficacy in tumor-infiltrating lymphocyte activation with synergistic gene editing

Authors: Nikolaos Memmos[1,2], Kamran Kaveh[2], Beau R. Webber[3], Branden S. Moriarity[3], David J. Odde[1,2*]

[1] University of Minnesota, Department of Biomedical Engineering, Minneapolis, Minnesota, USA.

[2] University of Minnesota, Therapy Modeling and Design Center, Minneapolis, Minnesota, USA.

[3] University of Minnesota, Department of Pediatrics, Minneapolis, Minnesota, USA.

* Corresponding author: oddex002@umn.edu

Abstract

Tumor-infiltrating lymphocyte (TIL) therapy is a type of adoptive cell therapy, where the lymphocytes of a cancer patient's tumor are harvested, expanded *in vitro* using IL-2 stimulation, and then infused back into the patient[1], [2]. However, even with the use of TIL therapy, cancer cells can survive for various reasons, such as poor lymphocyte infiltration into tumors, chronic activation of the T cell receptor and the immunosuppressive tumor microenvironment[3]. Cytokine-inducible SH2-containing (CISH) protein is a negative regulator of T cell activation, and in a recent clinical trial was knocked out in TILs to improve TIL therapy efficacy[4]. In this study, we developed a mechanistic signaling pathway model to theoretically evaluate the efficacy of *CISH* knockout (*CISH* KO) in T cell activation and examine potential alternative target genes that can theoretically be targeted using multiplex gene-editing or drugs to further improve T cell activation and function[5]. Our modeling results demonstrate that *CISH* knockout increases the transcription of activation biomarkers IL-2 and TNF-α, but also inhibitory biomarkers such PD1 and FasL. Using global sensitivity analysis, we also found that *GSK3B*, which is responsible for the deactivation of the NFAT, is also predicted to further increase T cell activation when knocked out. In addition, we predict that *PDCD1*, *FAS* and *CTLA4* can be knocked-out in combination with *CISH* to further enhance T cell activation and prevent exhaustion and apoptosis.

Introduction

Adoptive cell therapy (ACT) is a form of personalized cancer treatment that consists of harvesting immune cells, expanding them *in vitro* and transferring them back to the patient to

eliminate tumor cells[1]. There are two main approaches; one where immune cells are harvested directly from cancer patients to treat their own disease, i.e. autologous cell therapy, or another where immune cells are obtained from healthy donors, i.e. allogeneic cell therapy[6].

A major advancement in the efficacy of ACT was in 1976 when it was discovered that the administration of interleukin-2 (IL-2) can expand T cells *ex vivo*[2]. Moreover, Rosenberg *et al*. showed that high doses of IL-2 result in the generation of lymphokine-activated killer (LAK) cells that mediate the regression of tumors in mice[7]. Donohue *et al.* examined the effect of administration of IL-2 after adoptive cell transfer[8]. Despite their initial promising results in a clinical trial, where 11 of 25 patients with different types of metastatic cancer, including melanoma, colorectal, and renal-cell, showed tumor regression after the administration of LAK, a subsequent clinical trial did not demonstrate a statistically significant benefit compared to the administration of IL2 alone in patients with renal cell cancer[9], [10].

Tumor-infiltrating lymphocyte (TIL) therapy is a novel cancer immunotherapy that patient's own immune cells, present in the tumor microenvironment, are harvested, expanded *in vitro* and reinfused back to the patient to fight cancer. TILs after expansion with IL-2 showed 50 to 100 times higher efficacy compared to LAK cells in lung and hepatic metastatic tumors, although only with pretreatment with cyclophosphamide[11]. The first example of TIL therapy was in 1988, when Rosenberg *et al.* used autologous TILs along with the administration of IL-2 and pretreatment with cyclophosphamide to treat 20 patients with metastatic melanoma[12]. This study showed that the administration of TILs resulted in positive response in 9 out of 15 patients who were not treated with IL-2 before and in 2 of 5 who were treated with IL-2 in the past, compared to IL-2 and cyclophosphamide alone. A significant milestone in TIL therapy happened in 2002 when it was shown that the use of nonmyeloablative chemotherapy regimen as

conditioning to achieve lymphodepletion before TIL infusion in patients with metastatic melanoma causes tumor regression[13].

Neoantigen-reactive TIL therapy leverages the subset of tumor-infiltrating lymphocytes that are specific to the neoantigens expressed by tumor cells. Selection of neoantigen-reactive TIL pools can be accomplished using immunoassays to evaluate reactivity against candidate neoantigens nominated by next-generation sequencing of patient tumors[14]. Neoantigen-reactive TIL therapy has shown the potential to cure metastatic cancer. Zacharakis *et al.* presented the case of a patient with metastatic breast cancer who was treated with TILs specific to neoantigens created by nonsynonymous mutations in four genes, *SLC3A2, KIAA0368, CADPS2* and *CTSB*, and lead to complete regression that persisted for more than 22 months[15]. Tran *et al*. published a case report of a patient with metastatic colorectal cancer. The patient was treated with T cells that target a neoantigen created by KRAS G12D[16]. All seven metastatic sites in the lungs regressed but one of them relapsed after 9 months of therapy because of the loss of chromosome 6 that encoded HLA-C*08:02 protein, which is necessary for the T cells to recognize the KRAS G12D tumor antigen. In 2024, the FDA approved the first TIL therapy for patients with melanoma who have been treated before with PD1 inhibitor[17].

Despite the success of neoantigen-reactive TIL therapy, it is not yet the norm. Zacharakis *et al*. examined the efficacy of the therapy in conjunction with pembrolizumab in patients with metastatic breast cancer[18]. TILs were isolated from 42 patients but only 6 of them were found eligible to be treated. From these patients, only 1 had a complete response which persisted over 5.5 years, 2 partial responses at 6 and 10 months, and tumor regression in 3 patients. This may be attributed to the immunosuppressive properties of tumor microenvironment in solid tumors, for example the poor infiltration of lymphocytes, the expression checkpoint inhibitors, poor

neoantigen presentation and chronic T cell receptor (TCR) activation[3]. To counteract these effects, there have been intensive efforts to override the intrinsic checkpoints that limit T cell activation pathways.

Cytokine-inducible SH2-containing (CISH) protein is a member of suppressors of cytokine signaling (SOCS) family and a novel intracellular checkpoint[19]. It has been shown that all eight members of the SOCS family, which are SOCS1-7 and CISH, play a key role in immune regulation[19], [20], [21], [22], [23]. Delconte *et al.* observed that CISH protein is a negative regulator of IL-15 in natural killer cells, and its deletion increases sensitivity to IL-15[24]. The deletion of *CISH* also increased production of IFN-γ and cytotoxicity against tumors, because of its interaction with JAK1 protein in the JAK-STAT signaling pathway[19], [22], [23], [25], [26], [27]. Palmer *et al.* also demonstrated that CISH is responsible for the ubiquitination and degradation of PLC-γ1 in T cells after TCR activation[19]. *In vivo* experiments showed that knocking out CISH protein increased the activation of T cells by enhancing the translocation of NFAT and NFκB in the nucleus, while it also increased the phosphorylation of ERK which contributes to higher T cell activity[28]. These results led to the development of genetically engineered TILs using CRISPR/Cas9 *CISH* knockout, resulting in a human phase I/II clinical trial (NCT04426669) to treat metastatic gastrointestinal cancer[4].

Here, we present a modeling study where we examine whether *CISH* KO can theoretically increase the activation and function of T cells, and whether there are other genetic modifications that could be used instead of, or in combination with *CISH* KO to achieve maximal effect on T cell activation. A mechanistic model has been previously developed using ordinary differential equations (ODEs) that captures the effects of NFAT with respect to important biomarkers for T cell activation, such as IL-2, TNF-α, CTLA-4 and Fas ligand (FasL),

as described in Shin *et al*.[5]. Based on their model, we expanded it to include PD1, CISH, and PLCγ1 proteins, as well as more protein interactions, to capture the effect of *CISH* KO in T cell function. IL-2 and TNF-α are both responsible for the activation and expansion of T cells[29], [30], [31], [32]. In addition, TNF-α plays a major role in recruiting other immune cells in the tumor site[33], [34]. On the other hand, PD1 acts as an immune checkpoint to prevent the overactivation of T cells and contributes to T cell exhaustion, while inhibiting the activation of TCR, PI3K and Ras signaling[35], [36], [37]. Furthermore, CTLA-4 has an inhibitory action on T cells by competing with CD28 for binding to the B7 protein on antigen presenting cells (APCs) and it inhibits the action of PP2A[38], [39], [40]. The role of FasL is to maintain immune homeostasis by inducing activation-induced cell death (AICD) in T cells[41].

Our results predict that *CISH* KO will be highly effective in elevating the expression of both activation and inhibitory markers. Moreover, our results indicate that multiplex gene-editing of *CISH*, *PDCD1*, *FAS*, *CTLA4* may improve the efficacy of TILs, and also suggest that inhibition of GSK3β protein, which increases proliferation of T cells, could further improve T cell function in this context [42], [43], [44].

Model

The formulation of the CISH model developed here is based on the paper of Shin *et al*.[5], originally developed to study activation-induced cell death (AICD) in T cells. In our study, the Shin et al. model was modified to integrate PLCγ1, CISH and PD1 and their interactions with other proteins **(Figure 1**). Enzyme-catalyzed reactions and indirect cascade effects were modeled using Michaelis-Menten reaction kinetics. For example, calcineurin activation, which is triggered by calcium release in the cytosol through the endoplasmic

reticulum after the phosphorylation of PLCγ1, was simplified using a Michaelis-Menten equation (**Supplementary Table A.1,** reaction 6) to reduce model complexity. Similarly, the activation of TAK1, which is induced by TNF-α via tumor necrosis factor receptor (TNFR) was reduced to a single Michaelis-Menten equation (**Supplementary Table A.1**, reaction 43).

Moreover, the Michaelis-Menten equations were decomposed into a two-step reaction, comprising a reversible binding step ($E + S \leftrightarrow ES$) and an irreversible catalytic step ($ES \rightarrow E + P$), to enhance model stability during sensitivity analysis and maintain mass conservation. mRNA production rates were modeled as zeroth-order reactions (i.e. occurred at a constant rate), while degradation was modeled as a first-order reaction, with rates proportional to the concentration of the species being degraded. To account for the role of NFAT in protein transcription, Hill functions were used to describe the target gene mRNA expression dependence on NFAT. Mass-action kinetics were used to model association and dissociation events (**Supplementary Table A.1**).

The strength of the model of Shin *et al.* lies in its detailed representation of the feedback loops that are involved in the NFAT expression[5]. In addition, our model incorporates the NFAT-mediated feedback loop for CISH expression, wherein NFAT activation enhances CISH transcription, and subsequently it leads to the ubiquitination of PLCγ1. Additionally, the model includes the regulation of PD1 expression via the NFAT translocation to the nucleus and the inhibitory effect of PD1 protein to the TCR, Ras and PI3K signaling. Our model consists of 160 free parameters and 74 ODEs and uses the same initial conditions as the original Shin *et al*. model. For the rest of the species, they were assumed to be 10 nM for the free intracellular proteins, 0 nM for the protein complexes, 0.1 nM for the surface proteins (e.g. CTLA-4) and mRNAs. The model was implemented in the Julia programming language[45].

Methods

ODE solvers

The DifferentialEquations.jl package in Julia was utilized in this study, since it provides a wide range of ODE solvers[46]. To solve the ODE system, the QNDF or the Rosenbrock23 methods were used[46], [47], [48]. The Rosenbrock23 solver was paired with the Tsit5 solver using an auto-switching algorithm to enable the switching between these two solvers, based on the stiffness of the ODE system[49]. The QNDF solver was used during the parameter estimation step, while the Rosenbrock23/Tsit5 solvers were used during the global sensitivity analysis and steady-state simulations because of their ability to take larger time steps, thus reducing the computational cost[50]. To further improve computational efficiency during global sensitivity analysis and steady-state simulations, numerical differentiation with central differencing was implemented. For parameter estimation, automatic differentiation was employed, providing higher accuracy but at a greater computational cost[51].

Parameter estimation

Published *in vitro* experimental data were used to establish baseline parameter values [5], [39], [52], [53], [54], [55]. The lower and upper bounds of the parameter ranges are given in **Supplementary Table A.3**, while the estimated parameter values in **Supplementary Table A.4**. Because of large number of model parameters and the limited experimental data, many of the model parameters are non-identifiable[56]. To tackle this issue, Fides package for interior trust region reflective for boundary constrained optimization was used[57]. The objective function of the optimization problem is given by:

$$\pi(y|h,\sigma) = \frac{1}{\sqrt{2\sigma^2}} \exp\left(-\frac{(y-h)^2}{2\sigma^2}\right) \quad (1)$$

where y is the experimental measurement, h is the model observable and σ the standard deviation of the noise. A common problem in intracellular networks is the mismatch between the model outputs and the form of the experimental measurements, which in many cases are normalized or have different units. For this reason, a linear mapping between the observables and the experimental measurements was used[58]:

$$y = scale * h + offset \quad (2)$$

To estimate the gradient of the objective function with respect to the model parameters, forward automatic differentiation method was used. For computing the Hessian matrix, the Gauss-Newton method was used[59]. PEtab.jl library in the Julia programming language was used to implement parameter estimation[60]. The absolute and relative tolerances of the ODE solver were set to 10^{-3} and 10^{-6} respectively.

Global Sensitivity Analysis

To identify the sensitive parameters, the Morris method was used[61]. The Morris method is based on the calculation of elementary effects (EE), which are defined as:

$$EE_i = \frac{[Y(X_1, X_2, \dots, X_i + \Delta, \dots, X_\kappa) - Y(X_1, X_2, \dots, X_\kappa)]}{\Delta} \quad (3)$$

where Y is the output of the model, X_i, $i = 1, \dots, k$ are the parameters of the model and Δ is the step size, which takes values in $\{\frac{1}{p-1}, \dots, 1 - \frac{1}{p-1}\}$ and p is the number of grid points in the parameter hyperspace. To sample the parameter hyperspace, r trajectories of $k + 1$ points are created, with k elementary effects per trajectory, one for each parameter, and total $r(k + 1)$ sample points. The trajectories are selected from a superset of trajectories to have the biggest spread in the parameter space[62].

The Morris method estimates the following sensitivity measures; μ, μ^* and σ:

$$\mu_i = \frac{1}{r}\sum_{j=1}^{r} EE_i^j \quad (4)$$

$$\mu_i^* = \frac{1}{r}\sum_{j=1}^{r} |EE_i^j| \quad (5)$$

$$\sigma_i^2 = \frac{1}{r-1}\sum_{j=1}^{r} (EE_i^j - \mu)^2 \quad (6)$$

Both, μ and μ^* are the means of the elementary effects and the absolute values of them respectively, and they are used to assess the overall influence of a parameter, while σ^2 is the variance of the distribution of the elementary effects and measures the non-linear and interactions with other parameters. Compared to μ, the use of μ^*prevents from potentially cancelling effect between positive and negative effects in the cases of non-monotonic or interactions with other parameters, resulting.

Results

Model calibration

The model was calibrated using experimental time series data from multiple sources for CISH, PLCγ1, phosphorylated PLCγ1 (pPLCγ1), Akt1, phosphorylated MEK (pMEK), phosphorylated ERK (pERK), TNF-α, IL-2, mRNA coding for IL-2 (mIL-2), NFAT, PD1, CTLA-4, and phosphorylated TCR (pTCR)[5], [39], [52], [53], [54], [55]. In all instances, wild-type T cells were stimulated with anti-CD28 and anti-CD3 antibodies. The CISH, PLCγ1 and phosphorylated PLCγ1 data were extracted from western blots using Fiji Image software, while the remaining data were extracted using WebPlotDigitizer[63], [64]. The initial stimulation of the T cell was modeled as a rectangular pulse function with a 2-minute duration. Despite the large number of free parameters and the limited experimental data, Fides algorithm performed well in fitting the model to the experimental data. To estimate the parameters, 10000 starts from different initial points in the parameter space were used (**Supplementary Figure A.1**).

NFAT, IL-2, and mIL-2 displayed longer peaks in protein expression following TCR stimulation (**Figures 2A-C**), compared to pAkt, pMEK, pERK, and pPLCγ1, which all exhibited a rapid increase followed by a fast reduction in intracellular concentrations (**Figures 2D-F**, **Figure 2H**). In contrast, CISH and TNF-α concentrations demonstrated a consistent increase over time (**Figure 2I, 2K**). However, it is important to note that the datasets for CISH, PLCγ1, and pPLCγ1 contained only four data points at early time points, potentially limiting the ability of the model to make accurate predictions at later times. PD1 concentration displays a much slower decay rate compared to the rest (**Figure 2L**). Additionally, CTLA-4 exhibits an initial peak after TCR activation and then a decrease that leads to a persistent expression (**Figure 2J**).

The large number of model parameters and limited experimental data hinder the predictive power of the model due to identifiability and overfitting issues. In our case, parameter fitting is crucial for establishing baseline values for the intracellular biological processes that we

consider therapeutically unmodifiable, primarily the baseline generation and degradation rates of proteins and mRNAs, $kgen_i$ and $kdeg_i$, respectively (**Supplementary Table A.1**), which were held constant for the rest of the analysis. In the case of proteins that depend on the NFAT upregulation, CISH, RCAN, Carabin, CTLA-4 and PD1, and the expression of mRNA coding for NFAT, both the production rate of mRNAs and the proteins were considered as free parameters. Moreover, the Michaelis-Menten parameter, km_i, (**Supplementary Table A.1**) was kept constant based on the estimated values from the parameter fitting step. Using this approach, the number of free parameters was reduced from 160 to 71, which further reduced the computational cost of the sensitivity analysis. Furthermore, by limiting the number of free parameters during the rest of the analysis, we were able to obtain a better understanding of the important parts of the pathway.

Critical parts of the pathway

To identify if *CISH* is a good candidate for targeting and what other parts of the pathway can potentially be targeted independently or in conjunction with *CISH* KO, global sensitivity analysis (GSA) was performed using the Morris method. The outputs of Morris method are the μ_i^* (**Equation 5**), which measures the influence of each parameter, and σ_i^2 (**Equation 6**) that corresponds to the variance of the output with respect to parameter i, which corresponds to a nonlinear or interacting behavior of the parameter.

As an output for the sensitivity analysis, the steady-state concentrations of IL-2, TNF-α, PD1, FasL and CTLA-4 were used. It was assumed that T cells are, on average, in a continuously activated state in the tumor microenvironment[65], [66]. Compared to other global sensitivity analysis methods, for example Sobol, the Morris method is less accurate in terms of the ranking of the parameters, but because of the prohibitively high computational cost of the Sobol method

due to the number of free parameters and steady-state simulations, the Morris method was used for the purpose of this study.

The expression level of IL-2 protein exhibits high sensitivity to the production velocity of CISH (*v33*) and the deactivation of calcineurin, *v6a*, with values of μ^*_{v33} and μ^*_{v6a} equal to 3.36 and 3.14 respectively (**Figure 3A**). Furthermore, the high variances of v33 and v6a parameters indicate a possible interaction with other parameters. The production rate of PD1, *v35*, and the dephosphorylation rate of pGSK3β, *v27*, have a lower effect on IL-2 expression, but parameter v35 shows a high variance ($\sigma^2_{v35} = 142.9$), similar to the production velocity of mNFAT, *v6*, which corresponds to the positive self-feedback loop of NFAT regulation and has a high variance, with a value 186.29. A summary of the parameters and their meaning is shown in **Table 3.1**.

TNF-α is extremely sensitive to the deactivation of calcineurin, CISH production and dephosphorylation pGSK3β due to the high values of μ^*_i (**Figure 3B**), while the parameters also exhibit variances on the order of ~10^8. Furthermore, the parameters *v27*, *v6a* and *v33* appear to influence FasL, PD1 and CTLA-4 (**Figures 3C-E**). According to the sensitivity analysis, PD1 and FasL are susceptible to changes in CISH production, dephosphorylation rate of pGSK3β, and deactivation of calcineurin, but also these parameters probably interact with other parameters. On the other hand, CTLA-4 appears to be less sensitive to these parameters. In the case of CTLA-4, the dephosphorylation rate of *v27* shows a high variance, which stems from interactions with other parameters or non-linear effects. Parameter *v17*, which influences FasL and CTLA-4, corresponds to the production of CTLA-4. An important observation is parameter *v31*, which corresponds to phosphorylation of IL-2 receptor (IL2R), has a high variance in FasL and PD1

respectively (variances equal to $9.8*10^5$ and $2.6*10^4$), suggesting that the IL2R-PI3K-Rac1-Akt axis is potentially important.

Based on the global sensitivity analysis we confirm that theoretically *CISH* is an excellent target for genetic KO, via gene editing, as it is implicated in the expression of multiple distinct markers: *CISH* KO can increase the transcription of IL-2, TNF-α, PD1 and FasL. CTLA-4 is the most robust to parameter changes, compared to the other markers. Moreover, calcineurin appears to have an even more important role, since it directly acts on NFAT activation, while *PDCD1* and *GSK3B* gene-editing can also be used in conjunction with *CISH* knockout.

Efficacy of CISH KO

To analyze the long-term effects of *CISH* KO in T cells, 10000 cells were generated, under constant activation and with different parameter values, using sampling from a log-normal distribution with a mode equal to the fitted value of each parameter,

$$X \sim Lognormal(\mu, \sigma^2) \quad (7)$$

where μ and σ are the mean and the standard deviation of $\ln(X) \sim N(\mu, \sigma^2)$ distribution. The mode of the lognormal distribution is given by:

$$m = \exp(\mu - \sigma^2) \quad (8)$$

It was assumed that σ is equal to 0.8, thus all the sampled parameters will have the same coefficient of variation (CV=0.947), which is calculated based on the following equation:

$$CV = \sqrt{\exp(\sigma^2) - 1} \quad (9)$$

From the simulations, it observed that there is a large variability in the wild type T cells, with FasL exhibiting high expression in some cases and low expression in others. After knocking-out *CISH*, TNF-α and IL-2 increase, but also PD1, CTLA-4 and FasL, which is attributed to the rise of NFAT (**Figure 4**). This simultaneous rise in all markers can potentially explain the inability of *CISH* KO by itself to lead to tumor regression in mouse models of B16 melanoma[4], [28].

Therapy recommendations

As noted in Palmer *et al.*, *CISH* KO by itself was not sufficient to reduce tumor size in B16-melanoma bearing mice, but the combination of *CISH* KO and anti-PD1 block therapy had a high anti-tumoral efficacy[28]. Furthermore, Arthofer *et. al*. reported an increase in tumor cell killing after inactivation of both *CISH* and *PDCD1*[67]. In addition, the global sensitivity analysis of the model shows the dephosphorylation rate of pGSK3β to be important in some of these proteins. GSK3β is pivotal for deactivating NFAT via phosphorylation, since NFAT is inactivated when phosphorylated.

To test this in the model, the production rates of CISH and PD1 mRNAs, *v32* and *v35* respectively, were set equal to zero to simulate simultaneous knockout of *CISH* and *PDCD1* via multiplex gene editing[68]. In the case of simulated *GSK3B* knockout, both the initial conditions of GSK3β and pGSK3β were set to zero. Similarly to the previous section, 10000 cells for each case were simulated in a steady state. The synergistic inactivation of *CISH* and *PDCD1* lead to a higher expression of IL-2, compared to *CISH* KO alone, while *PDCD1* KO did not offer a

significant improvement, as the IL-2 concentration distribution in this case is similar to the wild type cells (**Figure 5A**), as was also shown by Cano *et al.*[69]. When GSK3β is knocked-out in combination with *CISH* and *PDCD1*, the production of IL-2 is increased as evidenced by the higher IL-2 concentrations in the distribution in this case. In addition to the increase of IL-2, the multiplex gene knockout of *CISH*, *PDCD1* and *GSK3B* results in a better outcome for TNF-α, confirming the observation from the sensitivity analysis that TNF-α is the most sensitive to these changes (**Figure 5B**). However, FasL increases significantly in *CISH* KO and the combinations of *CISH* KO + *PDCD1* KO or *CISH* KO + *PDCD1* KO + *GSK3B* KO have a modest effect (**Figure 5C**). CTLA-4 appears to increase significantly with the combination of *CISH* KO with *PDCD1* KO and *GSK3B* KO (**Figure 5D**).

According to these results, *CISH* KO leads to the biggest increase in the biomarkers, compared to the individual gene knockouts, since it acts directly on PLC-γ1 and it has been shown that PLC-γ1 deficiency in T cell impairs their activation upon TCR stimulation[70]. Our finding that CISH is an especially important negative regulator/checkpoint in T cell activation is consistent with recent experimental studies that similarly point to an especially important role for CISH[69]. CISH KO results in an increase in the transcription of IL-2 and TNF-α, with the latter being the most sensitive in this change. To improve therapeutic outcomes further, *PDCD1* and *GSK3B* can also be knocked-out to enhance T cell activity. Because of the increase of FasL expression, which can lead to AICD when it binds to Fas receptor (FasR), a combination of *CISH*, *PDCD1*, *GSK3B*, *CTLA4* and *FAS* knockout with multiplex gene-editing can be utilized to boost T cell reactivity, prevent exhaustion from PD1 and CTLA-4 and AICD from FasL. The benefits of targeting CTLA-4 and PD1 have been shown in numerous studies, including clinical trials[71], [72], [73], [74]. On the other hand, GSK3β is less popular as a potential target, despite

its role in the inhibition of T cell proliferation as a result of the phosphorylation of NFAT[42], [43]. Previous studies demonstrated that GSK3β inhibition led to better activation of T cells by downregulating PD1 and LAG3 proteins, while increasing the expression of transcriptional regulator TBET[44], [75], [76], [77], [78], [79], [80]. These effects appear to balance the reduced T cell motility after the inhibition of GSK3β[81].

Discussion

Adoptive cell therapy, such as TIL therapy, is an emerging form of cancer therapy that leverages antitumoral lymphocytes to fight against cancer cells, resulting in tumor regression or even eradication[1], [7], [8]. Neoantigen TIL therapies manage to mitigate this barrier with higher cancer cell specificity, as has been reported in cases like metastatic bladder and breast cancers[82]. Despite the progress, there are many other limiting factors, such as the tumor microenvironment, which leads to suppressed proliferation and migration of T cells, low expression of neoantigens and the major histocompatibility complex (MHC) on cancer cells[3].

Traditional checkpoint inhibitors, such as anti-PD1 and anti-CTLA-4 antibodies, have shown beneficial therapeutic outcomes, but the high patient and tumor variability of PD1 and CTLA-4 expressions limit their efficacy[67], [71], [74], [83], [84], [85], [86], [87], [88]. CISH protein is an intracellular checkpoint that is responsible for the ubiquitination of PLC-γ1 and multiple studies have reported that *CISH* knockout enhances TIL reactivity against cancer cells. Palmer *et al.* found that *CISH* knockout alone does not lead to tumor regression, because of the increase in PD1, whereas a combination of *CISH* knockout and anti-PD1 therapy resulted in tumor regression in mice[28]. In this study, we developed an ODE signaling pathway model to capture the roles of CISH and NFAT in T cell activation. Our model was based on the model of

Shin *et al.*, and modified to capture the effect of CISH in the expression of functional output biomarkers[5], including IL-2, TNF-α, PD1, CTLA-4 and FasL.

To estimate the parameters of the model, *in vitro* data from the literature have been used, where in all cases, T cells were stimulated with anti-CD28 and anti-CD3 antibodies to induce activation[5], [39], [53], [54], [55], [88]. There are significant differences in the transient behavior among the expression of proteins, for example NFAT and IL-2 exhibit a wider peak, compared to pAkt, pMEK, pERK, and pPLCγ1, which have a faster response followed by rapid decay. On the other hand, CISH and TNF-α increase over time, but in the case of CISH, we only had four data points in early times, thus we cannot be confident that this is the actual behavior at longer times post-activation. Furthermore, this limitation applies to pPLCγ1 and PLCγ1, while CTLA-4 expression exhibits an initial peak and then settles to a steady state value. Despite the limited amount of data for some of the outputs, the parameter estimation mostly served the purpose of establishing the baseline values for the protein degradation and generation rates, $kdeg_i$ and $kgen_i$ respectively, as well as the Michaelis-Menten constants, km_i.

To evaluate which parts of the pathway influence the outputs of the model the most, global sensitivity analysis was performed, using the Morris method[61]. The sensitivity analysis was used to find the most influential parameters with respect to the steady-state concentrations of IL-2, TNF-α, FasL, PD1 and CTLA-4, under constant stimulation of TCR. The estimated baseline parameters of $kdeg_i$, $kgen_i$ and km_i were kept constant during the global sensitivity analysis to gain a better understanding, since these parameters significantly influenced the outputs but do not contribute to improved insight into the biological mechanisms. From the analysis, it was concluded that *CISH* KO has a central role in the production of IL-2, TNF-α, CTLA-4, PD1 and FasL, and it potentially interacts with other parts of the pathway. An

important observation is the influence of GSK3β in expression of these proteins, indicating a possible additional target for multiplex gene-editing or drug targeting. GSK3β has been previously identified as a promising target for improving T cell activation, function and proliferation, despite the decrease in T cell migration[42], [43], [44], [81]. Furthermore, the steady-state simulations showed that CISH is the most crucial protein to target, but PD1 and GSK3β can also potentially be targeted, in conjunction with CISH targeting/knockout, to enhance TIL therapy effectiveness as well.

In conclusion, *CISH* KO is effective in increasing both activation and inhibitory markers. To compensate for the increase in inhibitory gene expression, a multiplex gene-editing approach is recommended where *CISH* is knocked-out in conjunction with knockout of *CTLA-4*, *PDCD1*, *FAS* and *GSK3B* to enhance T cell cytotoxicity and proliferation. The two most significant limitations of the current model are the limited experimental data that was used to calibrate the model and the focus on NFAT. A next step for improving the current model would be to collect more experimental time series data and include the NFκB transcription factor.

ACKNOWLEDGMENTS

B.R.W. acknowledges funding from Office of Discovery and Translation, NIH grants R21CA237789, R21AI163731, P01CA254849, P50CA136393, U54CA268069, R01AI146009, and Children's Cancer Research Fund. B.S.M. acknowledges funding from NIH grants R01AI146009, R01AI161017, P01CA254849, P50CA136393, U24OD026641, U54CA232561, P30CA077598, U54CA268069, Children's Cancer Research Fund, the Fanconi Anemia Research Fund, and the Randy Shaver Cancer and Community Fund. D.J.O. acknowledges funding support from NIH grants U54CA210190, U54CA268069, and P01CA254849.

Figures and Tables

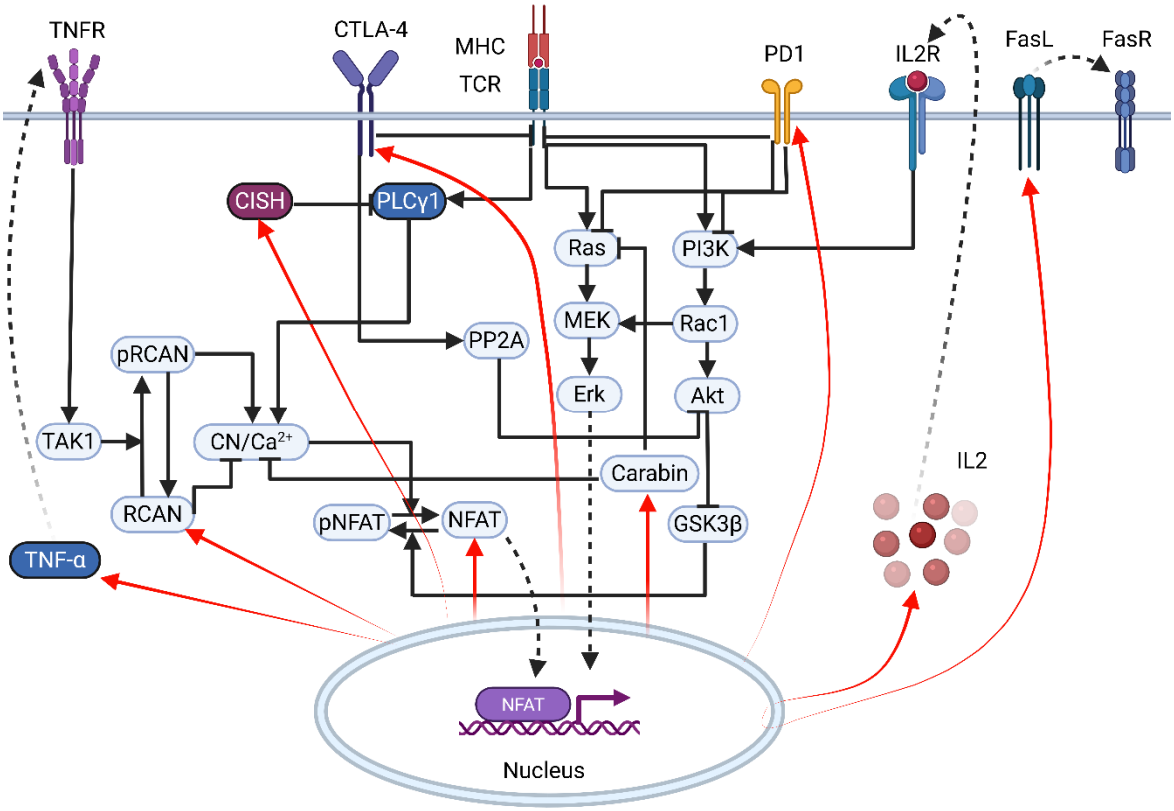

Figure 1. Model schematic for NFAT activation and downstream effects upon TCR activation. Black solid arrows and T-arrows indicate the activation and inhibition of proteins, respectively. Red arrows represent the expression of proteins that are dependent on NFAT transcription factor

acting in the nucleus. Dashed black arrows indicate the translocation of proteins to the nucleus or in the extracellular space.

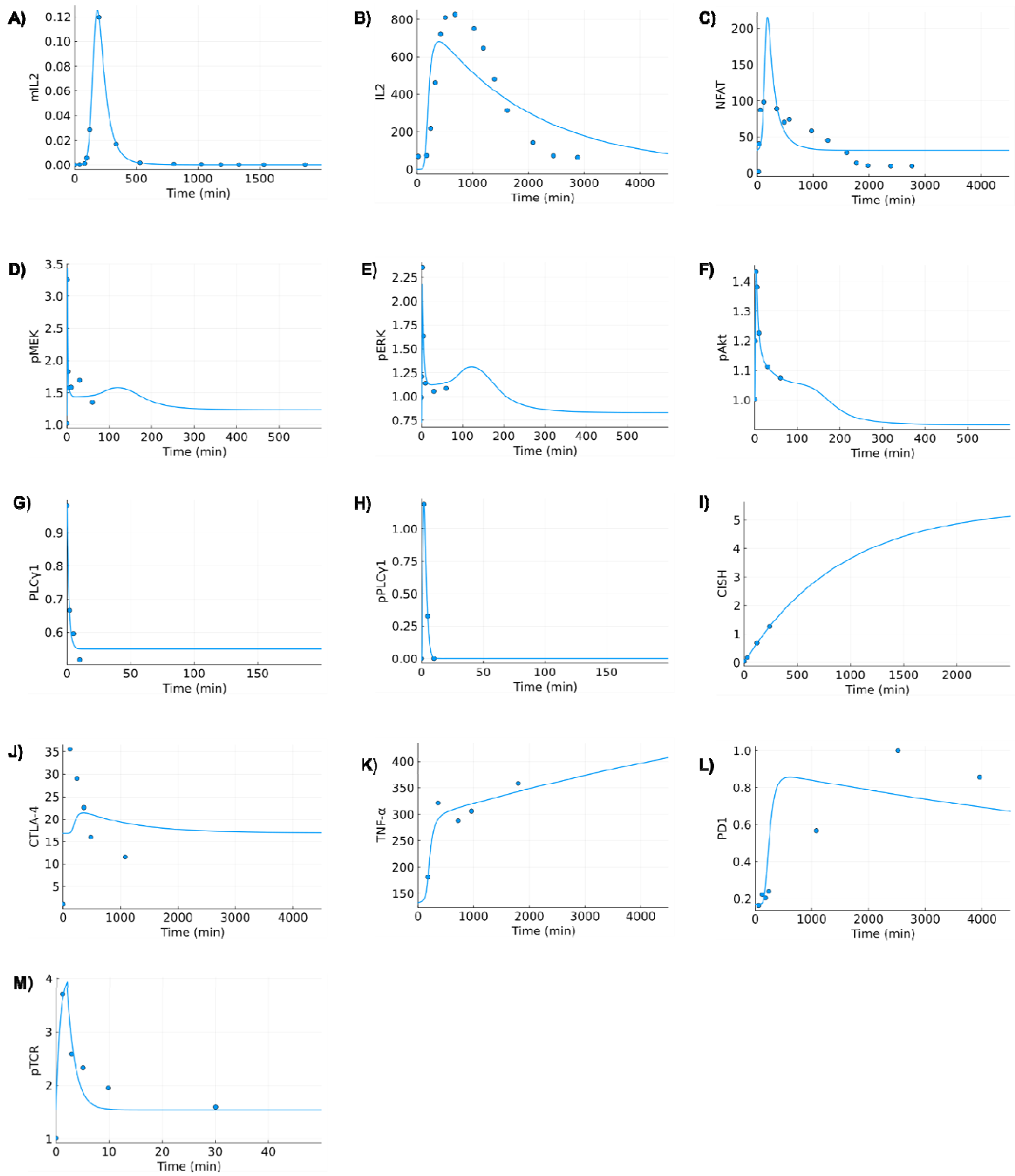

Figure 2. Model calibration based on 13 experimental outputs. The dots correspond to the experimental data obtained from references [5], [39], [52], [53], [54], [55] and the solid lines correspond to the model output. Equation (2) was used for the mapping between the model output and the experimental data.

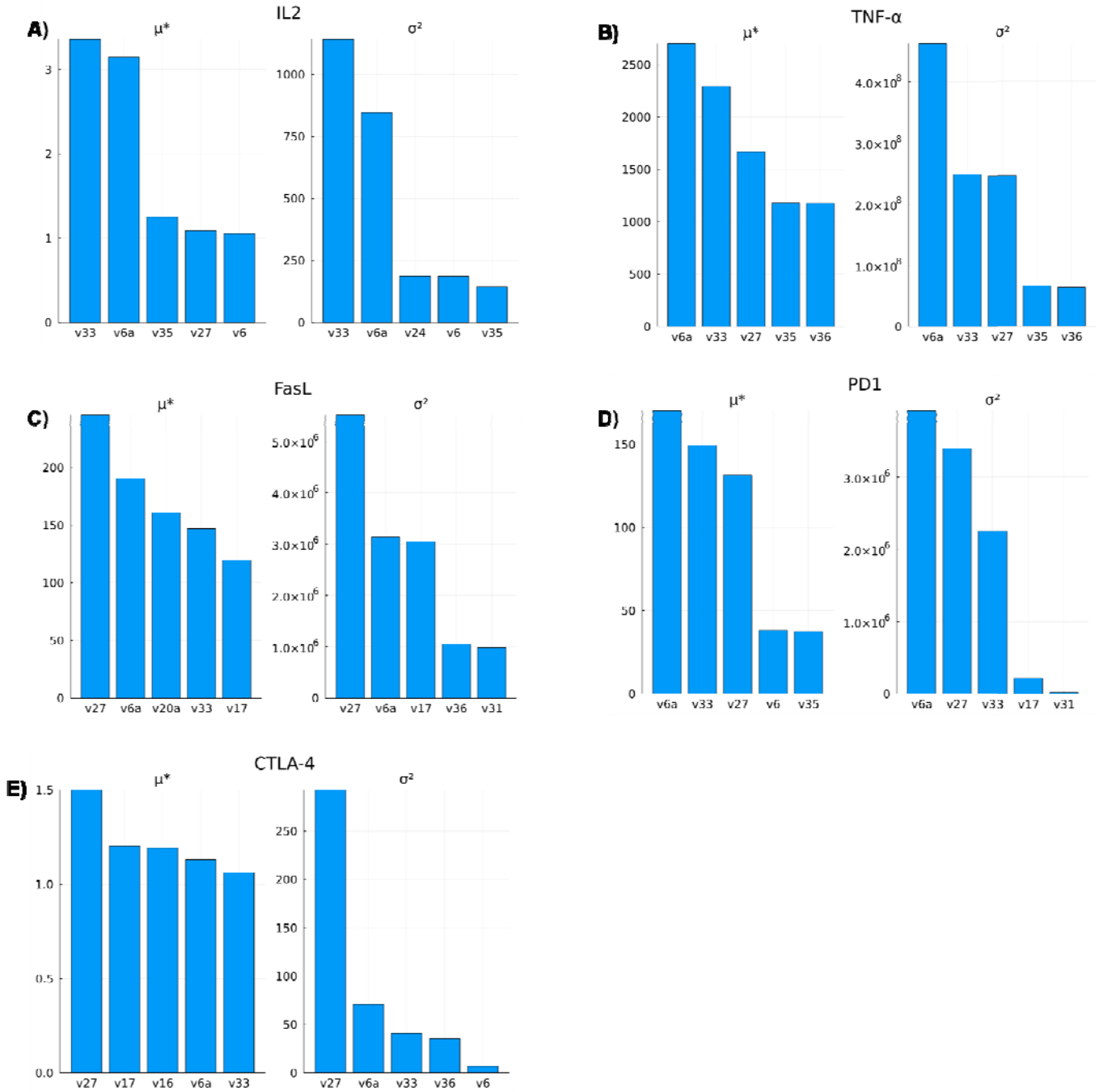

Figure 3. Parameter sensitivity analysis using the Morris method for **A)** IL-2, **B)** TNF-α, **C)** FasL, **D)** PD1 and **E)** CTLA-4 steady state concentrations under constant activation of the TCR. The mean, , is used to quantify the sensitivity of each output with respect to variations of a parameter, and the variance, , for the nonlinear behavior or interactions with other parameters.

Table 1. Sensitive parameters based on Morris global sensitivity analysis method and their biological meaning.

Parameter	**Meaning**
v33	Production of CISH protein
v6a	Deactivation of calcineurin
v35	Production of mPD1
v36	Production of PD1
v27	Dephosphorylation of pGSK3β
v6	Production of mNFAT
v24	Dephosphorylation of ERK
v20a	Production of FasL
v16	Production of mCTLA-4
v17	Production of CTLA-4
v31	Phosphorylation of inactive IL2R

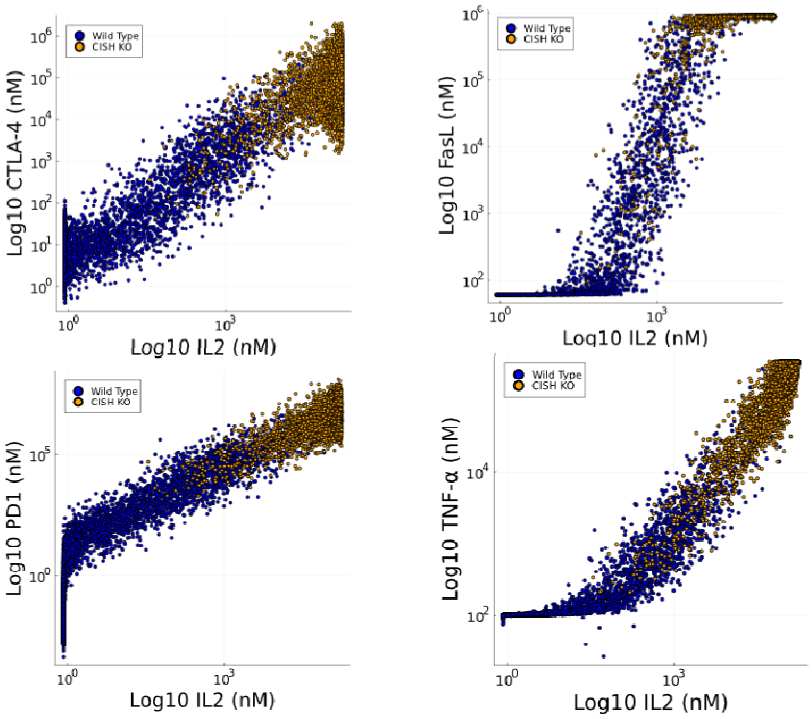

Figure 4. *In silico* steady state simulations for wild type and CISH KO T cells. CISH KO increases the expression of all markers. CISH KO increases the expression of IL-2, TNF-α, PD1, FasL and CTLA-4 simultaneously.

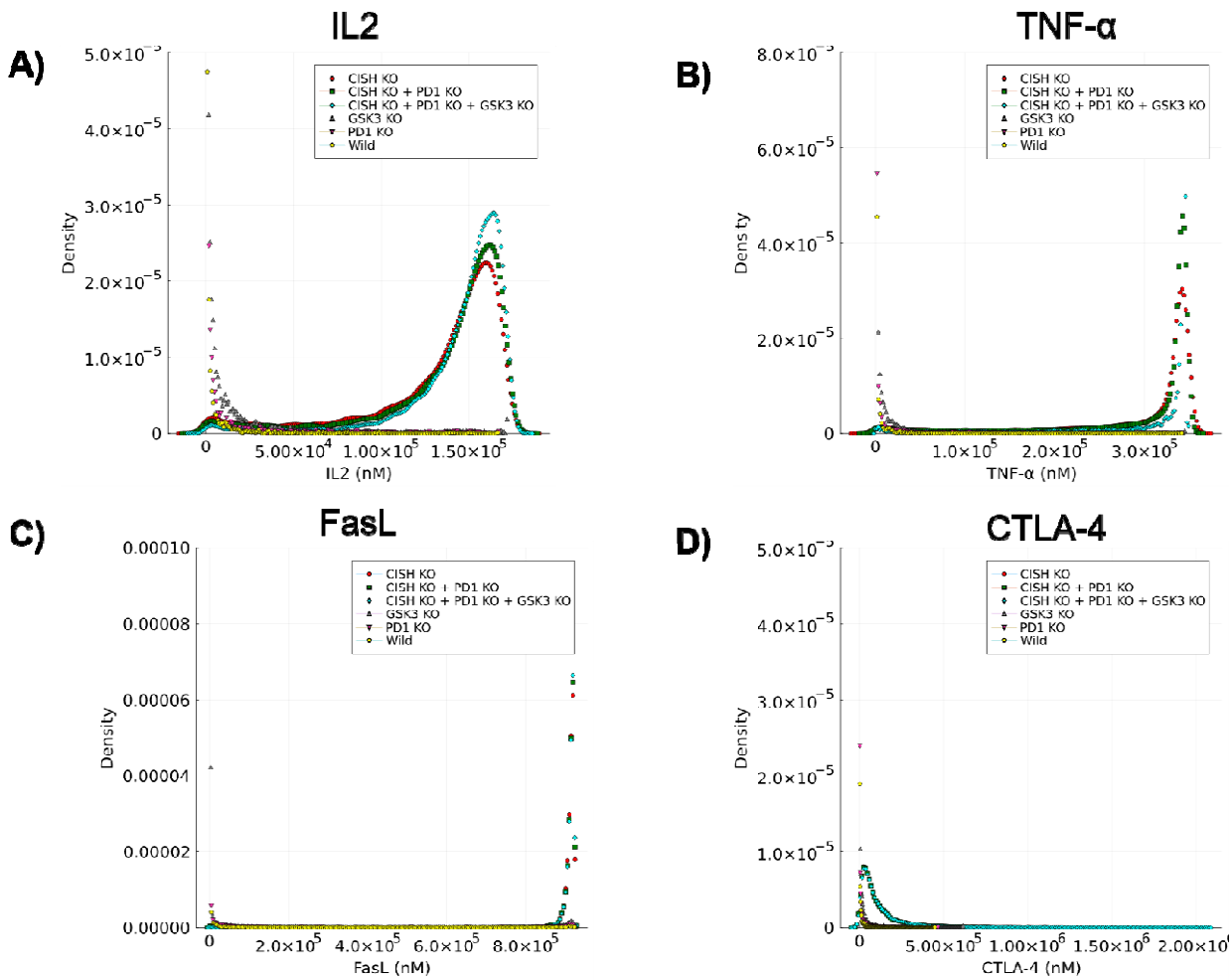

Figure 5. Steady-state concentration distributions of **A)** IL-2, **B)** TNF-α, **C)** FasL and **D)** CTLA-4 for different therapy combinations. CISH KO + PD1 KO + GSK3β KO leads to an increase in IL-2, TNF-α and FasL. CTLA-4 only requires CISH knockout to have higher expression, whereas the other outputs are further increased at steady-state by combining CISH KO with one or more other gene knockouts, such as PD1 and/or GSK3β.

References

[1] S. A. Rosenberg and N. P. Restifo, “Adoptive cell transfer as personalized immunotherapy for human cancer,” *Science (1979)*, vol. 348, no. 6230, pp. 62–68, Apr. 2015, doi: 10.1126/SCIENCE.AAA4967/ASSET/25CD0751-5C0D-4AE1-AB3E-242082A70CE0/ASSETS/GRAPHIC/348_62_F4.JPEG.

[2] D. A. Morgan, F. W. Ruscetti, and R. Gallo, “Selective in vitro growth of T lymphocytes from normal human bone marrows,” *Science*, vol. 193, no. 4257, pp. 1007–1008, 1976, doi: 10.1126/SCIENCE.181845.

[3] K. G. Anderson, I. M. Stromnes, and P. D. Greenberg, “Obstacles Posed by the Tumor Microenvironment to T cell Activity: A Case for Synergistic Therapies,” *Cancer Cell*, vol. 31, no. 3, pp. 311–325, Mar. 2017, doi: 10.1016/J.CCELL.2017.02.008/ASSET/0A6F3E9F-354F-4864-B90D-DD8E7617B493/MAIN.ASSETS/GR2.JPG.

[4] E. Lou *et al.*, “Targeting the intracellular immune checkpoint CISH with CRISPR-Cas9-edited T cells in patients with metastatic colorectal cancer: a first-in-human, single-centre, phase 1 trial,” *Lancet Oncol*, vol. 26, no. 5, pp. 559–570, May 2025, doi: 10.1016/S1470-2045(25)00083-X.

[5] S. Y. Shin, M. W. Kim, K. H. Cho, and L. K. Nguyen, “Coupled feedback regulation of nuclear factor of activated T-cells (NFAT) modulates activation-induced cell death of T cells,” *Sci Rep*, vol. 9, no. 1, p. 10637, Dec. 2019, doi: 10.1038/S41598-019-46592-Z.

[6] C. Bonini and A. Mondino, “Adoptive T-cell therapy for cancer: The era of engineered T cells,” *Eur J Immunol*, vol. 45, no. 9, pp. 2457–2469, Sep. 2015, doi: 10.1002/EJI.201545552.

[7] S. A. Rosenberg, J. J. Mulé, P. J. Spiess, C. M. Reichert, and S. L. Schwarz, “Regression of established pulmonary metastases and subcutaneous tumor mediated by the systemic administration of high-dose recombinant interleukin 2,” *J Exp Med*, vol. 161, no. 5, pp. 1169–1188, May 1985, doi: 10.1084/JEM.161.5.1169.

[8] J. H. Donohue, M. Rosenstein, A. E. Chang, M. T. Lotze, R. J. Robb, and S. A. Rosenberg, “The systemic administration of purified interleukin 2 enhances the ability of sensitized murine lymphocytes to cure a disseminated syngeneic lymphoma.,” *The Journal of Immunology*, vol. 132, no. 4, pp. 2123–2128, Apr. 1984, doi: 10.4049/JIMMUNOL.132.4.2123.

[9] S. A. Rosenberg *et al.*, “Observations on the systemic administration of autologous lymphokine-activated killer cells and recombinant interleukin-2 to patients with metastatic cancer,” *N Engl J Med*, vol. 313, no. 23, pp. 1485–1492, Dec. 1985, doi: 10.1056/NEJM198512053132327.

[10] S. A. Rosenberg *et al.*, “Prospective randomized trial of high-dose interleukin-2 alone or in conjunction with lymphokine-activated killer cells for the treatment of patients with

advanced cancer," *J Natl Cancer Inst*, vol. 85, no. 8, pp. 622–632, Apr. 1993, doi: 10.1093/JNCI/85.8.622.

[11] S. A. Rosenberg, P. Spiess, and R. Lafreniere, "A New Approach to the Adoptive Immunotherapy of Cancer with Tumor-Infiltrating Lymphocytes," *Science (1979)*, vol. 233, no. 4770, pp. 1318–1321, 1986, doi: 10.1126/SCIENCE.3489291.

[12] S. A. Rosenberg *et al.*, "Use of tumor-infiltrating lymphocytes and interleukin-2 in the immunotherapy of patients with metastatic melanoma. A preliminary report," *N Engl J Med*, vol. 319, no. 25, pp. 1676–1680, Dec. 1988, doi: 10.1056/NEJM198812223192527.

[13] M. E. Dudley *et al.*, "Cancer Regression and Autoimmunity in Patients After Clonal Repopulation with Antitumor Lymphocytes," *Science*, vol. 298, no. 5594, p. 850, Oct. 2002, doi: 10.1126/SCIENCE.1076514.

[14] P. F. Robbins *et al.*, "Mining exomic sequencing data to identify mutated antigens recognized by adoptively transferred tumor-reactive T cells," *Nat Med*, vol. 19, no. 6, pp. 747–752, Jun. 2013, doi: 10.1038/NM.3161,.

[15] N. Zacharakis *et al.*, "Immune recognition of somatic mutations leading to complete durable regression in metastatic breast cancer," *Nature Medicine 2018 24:6*, vol. 24, no. 6, pp. 724–730, Jun. 2018, doi: 10.1038/s41591-018-0040-8.

[16] E. Tran *et al.*, "T-Cell Transfer Therapy Targeting Mutant KRAS in Cancer," *New England Journal of Medicine*, vol. 375, no. 23, pp. 2255–2262, Dec. 2016, doi: 10.1056/NEJMOA1609279/SUPPL_FILE/NEJMOA1609279_DISCLOSURES.PDF.

[17] J. Chesney *et al.*, "Efficacy and safety of lifileucel, a one-time autologous tumor-infiltrating lymphocyte (TIL) cell therapy, in patients with advanced melanoma after progression on immune checkpoint inhibitors and targeted therapies: pooled analysis of consecutive cohorts of the C-144-01 study," *J Immunother Cancer*, vol. 10, no. 12, p. e005755, Dec. 2022, doi: 10.1136/JITC-2022-005755.

[18] N. Zacharakis *et al.*, "Breast Cancers Are Immunogenic: Immunologic Analyses and a Phase II Pilot Clinical Trial Using Mutation-Reactive Autologous Lymphocytes," *J Clin Oncol*, vol. 40, no. 16, pp. 1741–1754, Jun. 2022, doi: 10.1200/JCO.21.02170.

[19] D. C. Palmer *et al.*, "Cish actively silences TCR signaling in CD8+ T cells to maintain tumor tolerance," *Journal of Experimental Medicine*, vol. 212, no. 12, pp. 2095–2113, Nov. 2015, doi: 10.1084/JEM.20150304.

[20] D. J. Hilton *et al.*, "Twenty proteins containing a C-terminal SOCS box form five structural classes," *Proc Natl Acad Sci U S A*, vol. 95, no. 1, pp. 114–119, Jan. 1998, doi: 10.1073/PNAS.95.1.114.

[21] R. Starr *et al.*, "A family of cytokine-inducible inhibitors of signalling," *Nature 1997 387:6636*, vol. 387, no. 6636, pp. 917–921, Jun. 1997, doi: 10.1038/43206.

[22] T. A. Endo *et al.*, "A new protein containing an SH2 domain that inhibits JAK kinases," *Nature 1997 387:6636*, vol. 387, no. 6636, pp. 921–924, Jun. 1997, doi: 10.1038/43213.

[23] T. Naka *et al.*, "Structure and function of a new STAT-induced STAT inhibitor," *Nature 1997 387:6636*, vol. 387, no. 6636, pp. 924–929, Jun. 1997, doi: 10.1038/43219.

[24] R. B. Delconte *et al.*, "CIS is a potent checkpoint in NK cell-mediated tumor immunity," *Nat Immunol*, vol. 17, no. 7, pp. 816–824, Jun. 2016, doi: 10.1038/NI.3470.

[25] R. Morris, N. J. Kershaw, and J. J. Babon, “The molecular details of cytokine signaling via the JAK/STAT pathway,” *Protein Science*, vol. 27, no. 12, pp. 1984–2009, Dec. 2018, doi: 10.1002/PRO.3519.

[26] F. Verdier *et al.*, “Proteasomes Regulate Erythropoietin Receptor and Signal Transducer and Activator of Transcription 5 (STAT5) Activation: POSSIBLE INVOLVEMENT OF THE UBIQUITINATED CIS PROTEIN,” *Journal of Biological Chemistry*, vol. 273, no. 43, pp. 28185–28190, Oct. 1998, doi: 10.1074/JBC.273.43.28185.

[27] A. Matsumoto *et al.*, “Suppression of STAT5 functions in liver, mammary glands, and T cells in cytokine-inducible SH2-containing protein 1 transgenic mice,” *Mol Cell Biol*, vol. 19, no. 9, pp. 6396–6407, Sep. 1999, doi: 10.1128/MCB.19.9.6396.

[28] D. C. Palmer *et al.*, “Internal checkpoint regulates T cell neoantigen reactivity and susceptibility to PD1 blockade,” *Med (N Y)*, vol. 3, no. 10, pp. 682-704.e8, Oct. 2022, doi: 10.1016/J.MEDJ.2022.07.008.

[29] A. K. Mehta, D. T. Gracias, and M. Croft, “TNF Activity and T cells,” *Cytokine*, vol. 101, p. 14, Jan. 2016, doi: 10.1016/J.CYTO.2016.08.003.

[30] X. Chen, M. Bäumel, D. N. Männel, O. M. Z. Howard, and J. J. Oppenheim, “Interaction of TNF with TNF Receptor Type 2 Promotes Expansion and Function of Mouse CD4+CD25+ T Regulatory Cells,” *The Journal of Immunology*, vol. 179, no. 1, pp. 154–161, Jul. 2007, doi: 10.4049/JIMMUNOL.179.1.154.

[31] V. Niederlova, O. Tsyklauri, M. Kovar, and O. Stepanek, “IL-2-driven CD8+ T cell phenotypes: implications for immunotherapy,” *Trends Immunol*, vol. 44, no. 11, pp. 890–901, Nov. 2023, doi: 10.1016/J.IT.2023.09.003/ASSET/94B18407-EFBC-4066-B52A-82ED670C9C48/MAIN.ASSETS/GR4.JPG.

[32] S. H. Ross and D. A. Cantrell, “Signaling and Function of Interleukin-2 in T Lymphocytes,” *Annu Rev Immunol*, vol. 36, p. 411, Apr. 2018, doi: 10.1146/ANNUREV-IMMUNOL-042617-053352.

[33] L. B. Silva *et al.*, “The Role of TNF-α as a Proinflammatory Cytokine in Pathological Processes,” *Open Dent J*, vol. 13, no. 1, pp. 332–338, Oct. 2019, doi: 10.2174/1874210601913010332.

[34] B. L. Salomon, M. Leclerc, J. Tosello, E. Ronin, E. Piaggio, and J. L. Cohen, “Tumor necrosis factor α and regulatory T cells in oncoimmunology,” *Front Immunol*, vol. 9, no. MAR, p. 345465, Mar. 2018, doi: 10.3389/FIMMU.2018.00444/PDF.

[35] K. S. Rallis, C. R. T. Hillyar, M. Sideris, and J. K. Davies, “T-cell-based Immunotherapies for Haematological Cancers, Part A: A SWOT Analysis of Immune Checkpoint Inhibitors (ICIs) and Bispecific T-Cell Engagers (BiTEs),” *Anticancer Res*, vol. 41, no. 3, pp. 1123–1141, Mar. 2021, doi: 10.21873/ANTICANRES.14870.

[36] V. A. Boussiotis, “Molecular and Biochemical Aspects of the PD-1 Checkpoint Pathway,” *N Engl J Med*, vol. 375, no. 18, pp. 1767–1778, Nov. 2016, doi: 10.1056/NEJMRA1514296.

[37] L. Chen and D. B. Flies, “Molecular mechanisms of T cell co-stimulation and co-inhibition,” *Nat Rev Immunol*, vol. 13, no. 4, pp. 227–242, Apr. 2013, doi: 10.1038/NRI3405.

[38] X. Xu *et al.*, “CTLA4 depletes T cell endogenous and trogocytosed B7 ligands via cis-endocytosis,” *J Exp Med*, vol. 220, no. 7, p. e20221391, Jul. 2023, doi: 10.1084/JEM.20221391.

[39] H. M. Gibson *et al.*, “Induction of the CTLA-4 gene in human lymphocytes is dependent on NFAT binding the proximal promoter,” *J Immunol*, vol. 179, no. 6, pp. 3831–3840, Sep. 2007, doi: 10.4049/JIMMUNOL.179.6.3831.

[40] E. A. Wohlfert and R. B. Clark, “’Vive la Résistance!’--the PI3K-Akt pathway can determine target sensitivity to regulatory T cell suppression,” *Trends Immunol*, vol. 28, no. 4, pp. 154–160, Apr. 2007, doi: 10.1016/J.IT.2007.02.003.

[41] E. Volpe, M. Sambucci, L. Battistini, and G. Borsellino, “Fas–Fas Ligand: Checkpoint of T Cell Functions in Multiple Sclerosis,” *Front Immunol*, vol. 7, no. SEP, p. 382, Sep. 2016, doi: 10.3389/FIMMU.2016.00382.

[42] C. E. Rudd, “Upstream-downstream: CD28 co-signaling pathways and T cell function,” *Immunity*, vol. 4, no. 6, pp. 527–534, Jun. 1996, doi: 10.1016/S1074-7613(00)80479-3/ASSET/0BF4FBBD-43D6-470D-BD13-99F95091B6D1/MAIN.ASSETS/GR4.JPG.

[43] T. Ohteki *et al.*, “Negative Regulation of T Cell Proliferation and Interleukin 2 Production by the Serine Threonine Kinase Gsk-3,” *Journal of Experimental Medicine*, vol. 192, no. 1, pp. 99–104, Jul. 2000, doi: 10.1084/JEM.192.1.99.

[44] A. R. Crespo, S. G. Luna, B. Moës, A. Rodriguez, and C. E. Rudd, “The many faceted role of glycogen synthase kinase-3 (GSK-3) in T cells and cancer immunotherapy,” *J Cancer Biol*, vol. 5, no. 1, p. 11, Apr. 2024, doi: 10.46439/CANCERBIOLOGY.5.058.

[45] J. Bezanson, A. Edelman, S. Karpinski, and V. B. Shah, “Julia: A Fresh Approach to Numerical Computing,” *https://doi.org/10.1137/141000671*, vol. 59, no. 1, pp. 65–98, Feb. 2017, doi: 10.1137/141000671.

[46] C. Rackauckas and Q. Nie, “DifferentialEquations.jl – A Performant and Feature-Rich Ecosystem for Solving Differential Equations in Julia,” *J Open Res Softw*, vol. 5, no. 1, p. 15, May 2017, doi: 10.5334/JORS.151.

[47] A. Sandu, J. G. Verwer, J. G. Blom, E. J. Spee, G. R. Carmichael, and F. A. Potra, “Benchmarking stiff ode solvers for atmospheric chemistry problems II: Rosenbrock solvers,” *Atmos Environ*, vol. 31, no. 20, pp. 3459–3472, Oct. 1997, doi: 10.1016/S1352-2310(97)83212-8.

[48] L. F. Shampine and M. W. Reichelt, “The MATLAB ODE Suite,” *https://doi.org/10.1137/S1064827594276424*, vol. 18, no. 1, pp. 1–22, Jul. 2006, doi: 10.1137/S1064827594276424.

[49] C. Rackauckas and Q. Nie, “Confederated modular differential equation APIs for accelerated algorithm development and benchmarking,” *Advances in Engineering Software*, vol. 132, pp. 1–6, Jun. 2019, doi: 10.1016/J.ADVENGSOFT.2019.03.009.

[50] C. Tsitouras, “Runge–Kutta pairs of order 5(4) satisfying only the first column simplifying assumption,” *Computers & Mathematics with Applications*, vol. 62, no. 2, pp. 770–775, Jul. 2011, doi: 10.1016/J.CAMWA.2011.06.002.

[51] R. D. Neidinger, “Introduction to Automatic Differentiation and MATLAB Object-Oriented Programming,” *https://doi.org/10.1137/080743627*, vol. 52, no. 3, pp. 545–563, Aug. 2010, doi: 10.1137/080743627.

[52] R. D. Reitsema *et al.*, “Effect of age and sex on immune checkpoint expression and kinetics in human T cells,” *Immunity and Ageing*, vol. 17, no. 1, pp. 1–12, Dec. 2020, doi: 10.1186/S12979-020-00203-Y/FIGURES/7.

[53] P. K. Chattopadhyay, J. Yu, and M. Roederer, “A live-cell assay to detect antigen-specific CD4+ T cells with diverse cytokine profiles,” *Nature Medicine 2005 11:10*, vol. 11, no. 10, pp. 1113–1117, Sep. 2005, doi: 10.1038/nm1293.

[54] D. Lodygin *et al.*, “A combination of fluorescent NFAT and H2B sensors uncovers dynamics of T cell activation in real time during CNS autoimmunity,” *Nat Med*, vol. 19, no. 6, pp. 784–790, Jun. 2013, doi: 10.1038/NM.3182.

[55] M. E. Kalland, N. G. Oberprieler, T. Vang, K. Taskén, and K. M. Torgersen, “T cell-signaling network analysis reveals distinct differences between CD28 and CD2 costimulation responses in various subsets and in the MAPK pathway between resting and activated regulatory T cells,” *J Immunol*, vol. 187, no. 10, pp. 5233–5245, Nov. 2011, doi: 10.4049/JIMMUNOL.1101804.

[56] R. N. Gutenkunst, J. J. Waterfall, F. P. Casey, K. S. Brown, C. R. Myers, and J. P. Sethna, “Universally Sloppy Parameter Sensitivities in Systems Biology Models,” *PLoS Comput Biol*, vol. 3, no. 10, p. e189, 2007, doi: 10.1371/JOURNAL.PCBI.0030189.

[57] F. Fröhlich and P. K. Sorger, “Fides: Reliable trust-region optimization for parameter estimation of ordinary differential equation models,” *PLoS Comput Biol*, vol. 18, no. 7, p. e1010322, Jul. 2022, doi: 10.1371/JOURNAL.PCBI.1010322.

[58] L. Schmiester, Y. Schälte, F. Fröhlich, J. Hasenauer, and D. Weindl, “Efficient parameterization of large-scale dynamic models based on relative measurements,” *Bioinformatics*, vol. 36, no. 2, pp. 594–602, Jan. 2020, doi: 10.1093/BIOINFORMATICS/BTZ581.

[59] Å. Björck, “Numerical Methods for Least Squares Problems,” *Numerical Methods for Least Squares Problems*, Jan. 1996, doi: 10.1137/1.9781611971484.

[60] L. Schmiester *et al.*, “PEtab—Interoperable specification of parameter estimation problems in systems biology,” *PLoS Comput Biol*, vol. 17, no. 1, p. e1008646, Jan. 2021, doi: 10.1371/JOURNAL.PCBI.1008646.

[61] M. D. Morris, “Factorial sampling plans for preliminary computational experiments,” *Technometrics*, vol. 33, no. 2, pp. 161–174, 1991, doi: 10.1080/00401706.1991.10484804.

[62] A. Saltelli *et al.*, “Global sensitivity analysis: The primer,” *Global Sensitivity Analysis: The Primer*, pp. 1–292, Jan. 2008, doi: 10.1002/9780470725184.

[63] J. Schindelin *et al.*, “Fiji: an open-source platform for biological-image analysis,” *Nature Methods 2012 9:7*, vol. 9, no. 7, pp. 676–682, Jun. 2012, doi: 10.1038/nmeth.2019.

[64] “WebPlotDigitizer.” Accessed: Feb. 24, 2025. [Online]. Available: https://automeris.io/docs/#cite-webplotdigitizer

[65] N. E. Scharping *et al.*, “Mitochondrial stress induced by continuous stimulation under hypoxia rapidly drives T cell exhaustion,” *Nat Immunol*, vol. 22, no. 2, pp. 205–215, Feb. 2021, doi: 10.1038/S41590-020-00834-9,.

[66] D. R. Heintzman, E. L. Fisher, and J. C. Rathmell, “Microenvironmental influences on T cell immunity in cancer and inflammation,” *Cellular & Molecular Immunology 2022 19:3*, vol. 19, no. 3, pp. 316–326, Jan. 2022, doi: 10.1038/s41423-021-00833-2.

[67] E. Arthofer *et al.*, “Genetic editing of CISH enhances T cell effector programs independently of immune checkpoint cell surface ligand expression,” *bioRxiv*, p. 2021.08.17.456714, Aug. 2021, doi: 10.1101/2021.08.17.456714.

[68] B. R. Webber *et al.*, “Highly efficient multiplex human T cell engineering without double-strand breaks using Cas9 base editors,” *Nature Communications 2019 10:1*, vol. 10, no. 1, pp. 1–10, Nov. 2019, doi: 10.1038/s41467-019-13007-6.

[69] F. Cano *et al.*, “CISH, a novel intracellular immune checkpoint, in comparison and combination to existing and emerging cancer immune checkpoints,” *bioRxiv*, p. 2025.04.26.650767, Apr. 2025, doi: 10.1101/2025.04.26.650767.

[70] G. Fu *et al.*, “Phospholipase Cγ1 is essential for T cell development, activation, and tolerance,” *J Exp Med*, vol. 207, no. 2, p. 309, Feb. 2010, doi: 10.1084/JEM.20090880.

[71] S. Mok, D. A. Çobanoğlu, H. Liu, J. J. Mancuso, and J. P. Allison, “Post-immunotherapy CTLA-4 Ig treatment improves antitumor efficacy,” *Proc Natl Acad Sci U S A*, vol. 121, no. 27, p. e2404661121, Jul. 2024, doi: 10.1073/PNAS.2404661121/SUPPL_FILE/PNAS.2404661121.SAPP.PDF.

[72] A. Parvez *et al.*, “PD-1 and PD-L1: architects of immune symphony and immunotherapy breakthroughs in cancer treatment,” *Front Immunol*, vol. 14, p. 1296341, Dec. 2023, doi: 10.3389/FIMMU.2023.1296341/PDF.

[73] Y. Jiang, M. Chen, H. Nie, and Y. Yuan, “PD-1 and PD-L1 in cancer immunotherapy: clinical implications and future considerations,” *Hum Vaccin Immunother*, vol. 15, no. 5, p. 1111, May 2019, doi: 10.1080/21645515.2019.1571892.

[74] P. De Silva, M. Aiello, C. Gu-Trantien, E. Migliori, K. Willard-Gallo, and C. Solinas, “Targeting CTLA-4 in cancer: Is it the ideal companion for PD-1 blockade immunotherapy combinations?,” *Int J Cancer*, vol. 149, no. 1, pp. 31–41, Jul. 2021, doi: 10.1002/IJC.33415.

[75] A. Taylor, J. A. Harker, K. Chanthong, P. G. Stevenson, E. I. Zuniga, and C. E. Rudd, “Glycogen Synthase Kinase 3 Inactivation Drives T-bet-Mediated Downregulation of Co-receptor PD-1 to Enhance CD8(+) Cytolytic T Cell Responses,” *Immunity*, vol. 44, no. 2, pp. 274–286, Feb. 2016, doi: 10.1016/J.IMMUNI.2016.01.018.

[76] A. Taylor and C. E. Rudd, “Glycogen Synthase Kinase 3 Inactivation Compensates for the Lack of CD28 in the Priming of CD8+ Cytotoxic T-Cells: Implications for anti-PD-1 Immunotherapy,” *Front Immunol*, vol. 8, no. DEC, Dec. 2017, doi: 10.3389/FIMMU.2017.01653.

[77] J. Krueger, C. E. Rudd, and A. Taylor, “Glycogen synthase 3 (GSK-3) regulation of PD-1 expression and and its therapeutic implications,” *Semin Immunol*, vol. 42, Apr. 2019, doi: 10.1016/J.SMIM.2019.101295.

[78] A. Taylor, D. Rothstein, and C. E. Rudd, “Small-Molecule Inhibition of PD-1 Transcription Is an Effective Alternative to Antibody Blockade in Cancer Therapy,” *Cancer Res*, vol. 78, no. 3, pp. 706–717, Feb. 2018, doi: 10.1158/0008-5472.CAN-17-0491.

[79] A. Taylor, J. A. Harker, K. Chanthong, P. G. Stevenson, E. I. Zuniga, and C. E. Rudd, “Glycogen Synthase Kinase 3 Inactivation Drives T-bet-Mediated Downregulation of Co-receptor PD-1 to Enhance CD8(+) Cytolytic T Cell Responses,” *Immunity*, vol. 44, no. 2, pp. 274–286, Feb. 2016, doi: 10.1016/J.IMMUNI.2016.01.018.

[80] C. E. Rudd, K. Chanthong, and A. Taylor, “Small Molecule Inhibition of GSK-3 Specifically Inhibits the Transcription of Inhibitory Co-receptor LAG-3 for Enhanced Anti-tumor Immunity,” *Cell Rep*, vol. 30, no. 7, pp. 2075-2082.e4, Feb. 2020, doi: 10.1016/J.CELREP.2020.01.076.

[81] A. Taylor and C. E. Rudd, “Glycogen synthase kinase 3 (GSK-3) controls T-cell motility and interactions with antigen presenting cells,” *BMC Res Notes*, vol. 13, no. 1, p. 163, Mar. 2020, doi: 10.1186/S13104-020-04971-0.

[82] Z. Zhang *et al.*, “Neoantigen: A New Breakthrough in Tumor Immunotherapy,” *Front Immunol*, vol. 12, p. 672356, Apr. 2021, doi: 10.3389/FIMMU.2021.672356/BIBTEX.

[83] N. Krishnamurthy *et al.*, “High CTLA-4 transcriptomic expression correlates with high expression of other checkpoints and with immunotherapy outcome,” *Ther Adv Med Oncol*, vol. 16, p. 17588359231220510, Jan. 2024, doi: 10.1177/17588359231220510.

[84] Y. Gonzalez-Montes *et al.*, “Genetic variants of CTLA4 are associated with clinical outcome of patients with multiple myeloma,” *Front Immunol*, vol. 14, p. 1158105, 2023, doi: 10.3389/FIMMU.2023.1158105/FULL.

[85] A. A. Davis and V. G. Patel, “The role of PD-L1 expression as a predictive biomarker: an analysis of all US Food and Drug Administration (FDA) approvals of immune checkpoint inhibitors,” *J Immunother Cancer*, vol. 7, no. 1, p. 278, Dec. 2019, doi: 10.1186/S40425-019-0768-9.

[86] K. Pawelczyk *et al.*, “Role of PD-L1 Expression in Non-Small Cell Lung Cancer and Their Prognostic Significance according to Clinicopathological Factors and Diagnostic Markers,” *Int J Mol Sci*, vol. 20, no. 4, Feb. 2019, doi: 10.3390/IJMS20040824.

[87] J. Lee *et al.*, “Outstanding clinical efficacy of PD-1/PD-L1 inhibitors for pulmonary pleomorphic carcinoma,” *Eur J Cancer*, vol. 132, pp. 150–158, Jun. 2020, doi: 10.1016/J.EJCA.2020.03.029.

[88] A. Martín-Ruiz *et al.*, “Effects of anti-PD-1 immunotherapy on tumor regression: insights from a patient-derived xenograft model,” *Sci Rep*, vol. 10, no. 1, Dec. 2020, doi: 10.1038/S41598-020-63796-W.

[89] B. Jones, D. Stekel, J. Rowe, and C. Fernando, “Is there a liquid state machine in the bacterium Escherichia coli?,” *Proceedings of the 2007 IEEE Symposium on Artificial Life, CI-ALife 2007*, pp. 187–191, 2007, doi: 10.1109/ALIFE.2007.367795.

[90] H. Chen, K. Shiroguchi, H. Ge, and X. S. Xie, “Genome-wide study of mRNA degradation and transcript elongation in Escherichia coli,” *Mol Syst Biol*, vol. 11, no. 1, p. 781, Jan. 2015, doi: 10.15252/MSB.20145794.

[91] S. Kühner *et al.*, “Proteome organization in a genome-reduced bacterium,” *Science (1979)*, vol. 326, no. 5957, pp. 1235–1240, Nov. 2009, doi: 10.1126/SCIENCE.1176343/SUPPL_FILE/KUEHNER.SOM.PDF.

[92] J.-M. Anaya, Y. Shoenfeld, A. Rojas-Villarraga, R. A. Levy, and R. Cervera, “Autoimmunity,” *Autoimmunity: From Bench to Bedside*, pp. 237–378, Jul. 2013, Accessed: Jun. 11, 2025. [Online]. Available: https://www.ncbi.nlm.nih.gov/books/NBK459447/

[93] D. Davidia *et al.*, “Global characterization of in vivo enzyme catalytic rates and their correspondence to in vitro kcat measurements,” *Proc Natl Acad Sci U S A*, vol. 113, no. 12, pp. 3401–3406, Mar. 2016, doi: 10.1073/PNAS.1514240113/SUPPL_FILE/PNAS.1514240113.SD01.XLSX.

[94] Y. Wang, C. L. Liu, J. D. Storey, R. J. Tibshirani, D. Herschlag, and P. O. Brown, “Precision and functional specificity in mRNA decay,” *Proc Natl Acad Sci U S A*, vol. 99, no. 9, pp. 5860–5865, Apr. 2002, doi: 10.1073/PNAS.092538799,.

[95] S. B. Cambridge, F. Gnad, C. Nguyen, J. L. Bermejo, M. Krüger, and M. Mann, "Systems-wide proteomic analysis in mammalian cells reveals conserved, functional protein turnover," *J Proteome Res*, vol. 10, no. 12, pp. 5275–5284, Dec. 2011, doi: 10.1021/PR101183K/SUPPL_FILE/PR101183K_SI_002.XLS.

Supplementary Information

To estimate the baseline generation rates for mRNAs, we assumed that the average mRNA length is 1000 nucleotides, the maximum elongation rate 70 nt/s and the average number of RNA polymerases[89], [90], [91] in a T-cell is 300. Moreover, it was assumed that the diameter of a T-cell is 10 μm, thus its volume is equal to – μm^3[92].

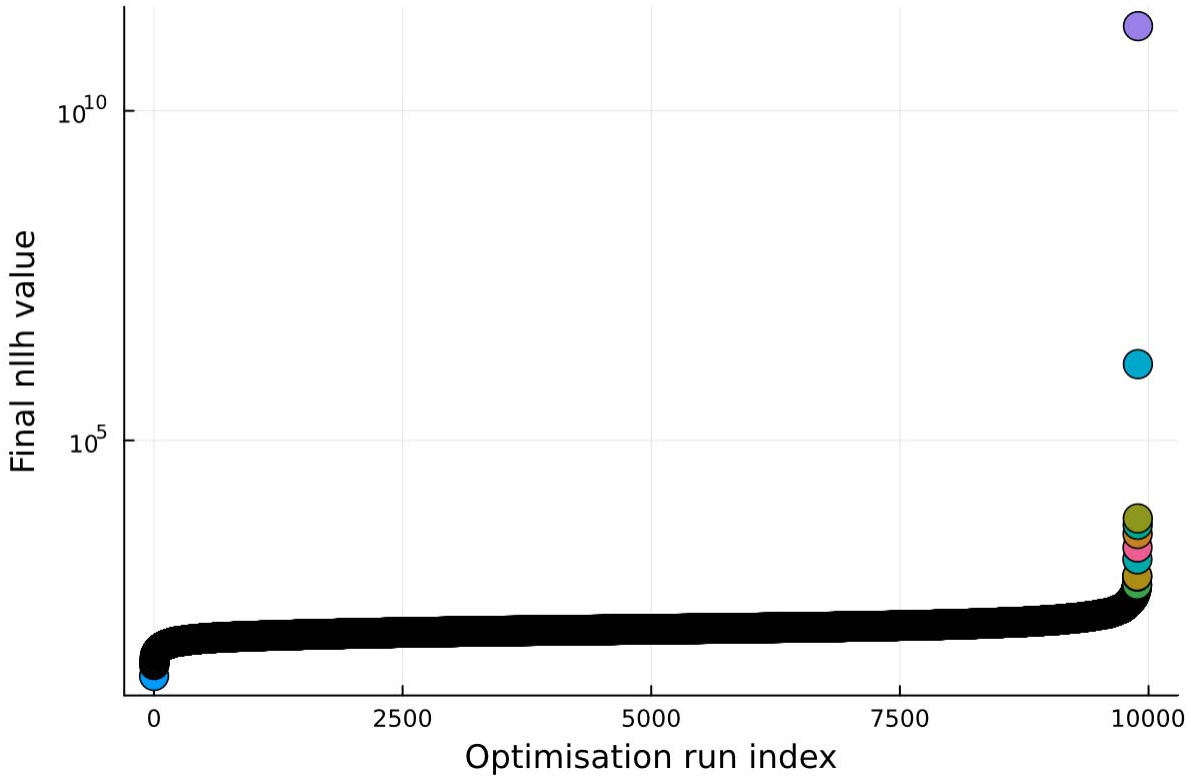

Figure A. 1. Waterfall plot for 10000 parameter estimations with different initial parameter values. The ranking is from the best on the left to the worst on the right on the x-axis. The y-axis corresponds to the negative log-likelihood, calculated based on (1).

Table A. 1. Table of reaction rates for CISH model.

No	Reaction	Reaction Rates
re_1	TCR → pTCR	kc1*E1*TCR/(km1+TCR)
re_2	pTCR + CTLA4 → TCR + CTLA4	kc2*(CTLA4)*pTCR/(km2+pTCR)
re_4	pTCR → iTCR	v3*pTCR/(km3+pTCR)
re_5	iTCR → TCR	v4*iTCR/(km4+iTCR)
re_6	CN → aCN	kc5a*pPLCg*CN/(km5a+CN)
re_7	aCN → CN	v6a*aCN/(km6a+aCN)
re_8	aCN+RCAN ↔ aCN_RCAN	kon*aCN*RCAN – kon*KD4*aCN_RCAN
re_9	aCN+pRCAN ↔ aCN_pRCAN	kon*aCN*pRCAN – kon*KD5*aCN_pRCAN
re_10	aCN+Carabin ↔ aCN_Carabin	kon*aCN*Carabin – kon*KD6*aCN_Carabin
re_11	pNFAT + aCN ↔ pNFAT_aCN	kon* pNFAT*aCN – kon*KD7*pNFAT_aCN
re_12	pNFAT_aCN → NFAT + aCN	kp2*pNFAT_aCN
re_13	pNFAT + aCN_pRCAN ↔ pNFAT_aCN_pRCAN	kon* pNFAT *aCN_pRCAN – kon*KD8* pNFAT_aCN_pRCAN
re_14	pNFAT_aCN_pRCAN → NFAT + aCN_pRCAN	kp3*pNFAT_aCN_pRCAN
re_15	NFAT → pNFAT	v5*NFAT/(km5 + NFAT)
re_16	NFAT + GSK3 ↔ NFAT_GSK3	kon*pNFAT*GSK3 – kon*KD9*NFAT_GSK3
re_17	NFAT_GSK3 → pNFAT + GSK3	kp4*NFAT_GSK3
re_18	∅ → mNFAT	kgen1
re_19	∅ → mNFAT	v6*NFAT/(km6+NFAT)
re_20	mNFAT → ∅	kdeg1*mNFAT
re_21	∅ → NFAT	v7*mNFAT/(km7+mNFAT)
re_22	NFAT → ∅	kdeg2*NFAT
re_23	pNFAT → ∅	kdeg3*pNFAT

re_24	∅ → mRCAN	kgen2
re_25	∅ → mRCAN	v8*NFAT^2/(km8^2+NFAT^2)
re_26	mRCAN → ∅	kdeg4*mRCAN
re_27	∅ → RCAN	v9*mRCAN/(km9+mRCAN)
re_28	RCAN → ∅	kdeg5*RCAN
re_29	RCAN + pTAK1 ↔ RCAN_pTAK1	kon*RCAN*pTAK1 – kon*KD10* RCAN_pTAK1
re_30	RCAN_pTAK1 → pRCAN + pTAK1	kp5* RCAN_pTAK1
re_31	pRCAN → RCAN	v10*pRCAN/(km10+pRCAN)
re_32	∅ → mCarabin	kgen3
re_33	∅ → mCarabin	v11*NFAT^2/(km11^2+NFAT^2)
re_34	mCarabin → ∅	kdeg6*mCarabin
re_35	∅ → Carabin	v12*mCarabin/(km12+mCarabin)
re_36	Carabin → ∅	kdeg7*Carabin
re_37	∅ → mTNFa	kgen4
re_38	∅ → mTNFa	v13*NFAT^2/(km13^2+NFAT^2)
re_39	mTNFa → ∅	kdeg8*mTNFa
re_40	∅ → TNFa	v14*mTNFa/(km14+mTNFa)
re_41	TNFa → ∅	kdeg9*TNFa
re_42	TAK1 → pTAK1	v15*pTAK1/(km15+pTAK1)
re_43	pTAK1 → TAK1	kc38*TAK1*TNFa/(km38 + TAK1)
re_44	∅ → mCTLA4	kgen5
re_45	∅ → mCTLA4	v16*NFAT^2/(km16^2+NFAT^2)
re_46	mCTLA4 → ∅	kdeg10*mCTLA4
re_47	∅ → CTLA4	v17*mCTLA4/(km17+mCTLA4)
re_48	CTLA4 → ∅	kdeg11*CTLA4
re_49	∅ → mIL2	kgen6
re_50	∅ → mIL2	v18a*(1+v18b*pERK/(km18b+pERK))*NFAT^2/(km18^2+NFAT^2)
re_51	mIL2 → ∅	kdeg12*mIL2
re_52	∅ → IL2	v19*mIL2/(km19+mIL2)
re_53	IL2 → ∅	kdeg13*IL2
re_54	∅ → mFasL	kgen7
re_55	∅ → mFasL	v20a*(1+v20b*pERK/(km20b+pERK))*NFAT^5/(km20^5+NFAT^5)
re_56	mFasL → ∅	kdeg14*mFasL
re_57	∅ → FasL	v21*mFasL/(km21+mFasL)
re_58	FasL → ∅	kdeg15*FasL
re_59	Ras → aRas	kc39*Ras*pPLCg/(km39 + Ras)
re_60	aRas → Ras	v22*aRas/(km22+aRas)
re_61	Carabin + aRas ↔ aRas_Carabin	kon*aRas*Carabin – KD13*kon*aRas_Carabin

re_62	MEK + aRas ↔ aRas_MEK	kon*aRas*MEK – KD14*kon*aRas_MEK
re_63	aRas_MEK → pMEK + aRas	kp8*aRas_MEK
re_64	MEK + Rac1GTP ↔ Rac1GTP_MEK	kon*Rac1GTP *MEK – KD15*kon*Rac1GTP_MEK
re_65	Rac1GTP_MEK → pMEK + Rac1GTP	kp9*Rac1GTP_MEK
re_66	pMEK → MEK	v23*pMEK/(km23+pMEK)
re_67	ERK + pMEK ↔ pMEK_ERK	kon* ERK*pMEK – KD16*kon*pMEK_ERK
re_68	pMEK_ERK → pMEK + pERK	kp10*pMEK_ERK
re_69	pERK → ERK	v24*pERK/(km24+pERK)
re_70	PI3K + pIL2R ↔ PI3K_pIL2R	kon*PI3K*pIL2R – KD17*kon*PI3K_pIL2R
re_71	PI3K_pIL2R → aPI3K + pIL2R	kp11*PI3K_pIL2R
re_72	PI3K + pTCR ↔ PI3K_pTCR	kon*PI3K * pTCR – KD18*kon*PI3K_pTCR
re_73	PI3K_pTCR → aPI3K + pTCR	kp12*PI3K_pTCR
re_74	aPI3K → PI3K	v25*aPI3K/(km25+aPI3K)
re_75	PP2A + CTLA4 ↔ PP2A_CTLA4	kon*PP2A*CTLA4 – KD19*kon*PP2A_CTLA4
re_76	PP2A_CTLA4 → aPP2A + CTLA4	kp13*PP2A_CTLA4
re_77	aPP2A → PP2A	v26*aPP2A/(km26+aPP2A)
re_78	Akt + aPI3K ↔ Akt_aPI3K	kon*Akt*aPI3K – KD20*kon*Akt_aPI3K
re_79	Akt_aPI3K → pAkt + aPI3K	kp14*Akt_aPI3K
re_80	pAkt + aPP2A ↔ pAkt_aPP2A	kon*pAkt*aPP2A – KD21*kon*pAkt_aPP2A
re_81	pAkt_aPP2A → Akt + aPP2A	kp15*pAkt_aPP2A
re_82	GSK3 + pAkt ↔ GSK3_pAkt	kon* pAkt *GSK3 – KD22*kon*GSK3_pAkt
re_83	GSK3_pAkt → pGSK3 + pAkt	kp16*GSK3_pAkt
re_84	pGSK3 → GSK3	v27*pGSK3/(km27+pGSK3)
re_85	Rac1GDP + aPI3K ↔ Rac1GDP_aPI3K	kon*Rac1GDP*aPI3K – KD23*kon* Rac1GDP_aPI3K
re_86	Rac1GDP_aPI3K →	kp17*Rac1GDP_aPI3K

	Rac1GTP + aPI3K	
re_87	Rac1GTP → Rac1GDP	v28*Rac1GTP/(km28+Rac1GTP)
re_88	IL2R + IL2 ↔ IL2R_IL2	kon*IL2R*IL2 – KD24*kon* IL2R_IL2
re_89	IL2R_IL2 → pIL2R + IL2	kp18* IL2R_IL2
re_90	pIL2R → IL2R	v29*pIL2R/(km29+pIL2R)
re_91	pIL2R → iIL2R	v30*pIL2R/(km30+pIL2R)
re_92	iIL2R → pIL2R	v31*iIL2R/(km31+iIL2R)
re_93	∅ → mCISH	v32*NFAT^2/(km32^2+NFAT^2)
re_94	∅ → mCISH	kgen8
re_95	mCISH → ∅	kdeg16*mCISH
re_96	∅ → CISH	v33*mCISH /(km33 + mCISH)
re_97	CISH → ∅	kdeg17*CISH
re_98	∅ → mPLCγ	kgen9
re_99	mPLCγ → ∅	kdeg18*mPLCγ
re_100	∅ → PLCγ	v34*mPLCγ /(km34 + mPLCγ)
re_101	PLCγ → ∅	kdeg19*PLCγ
re_102	PLCγ + pTCR ↔ PLCγ_pTCR	kon*PLCγ*pTCR – KD25*kon*PLCγ_pTCR
re_103	PLCγ_pTCR → aPLCγ + pTCR	kp19*PLCγ_pTCR
re_104	aPLCγ + CISH ↔ aPLCγ_CISH	kon*aPLCγ*CISH – KD26*kon*aPLCγ_CISH
re_105	aPLCγ_CISH → uPLCγ + CISH	kp20*aPLCγ_CISH
re_106	uPLCγ → ∅	kdeg20*uPLCγ
re_107	∅ → mPD1	v35*NFAT^2/(km35^2 + NFAT^2)
re_108	mPD1 → ∅	kdeg21* mPD1
re_109	∅ → PD1	v36*mPD1*(km36 + mPD1)
re_110	PD1 → ∅	kdeg22* PD1
re_111	pTCR + PD1 → TCR + PD1	kc37*(PD1)*pTCR/(km37+pTCR)
re_112	aRas + PD1 ↔ aRas_PD1	kon*aRas*PD1 – KD28*kon*aRas_PD1
re_113	aRas_PD1 → Ras + PD1	kp22*aRas_PD1
re_114	aPI3K + PD1 ↔ aPI3K_PD1	kon*aPI3K*PD1 – KD29*kon*aPI3K_PD1
re_115	aPI3K _PD1 → PI3K + PD1	kp23*aPI3K_PD1

It is assumed that the receptors TCR, CTLA-4, PD1 and IL2R have different binding motifs for different proteins, so the reactions with blue color do not affect the mass balance for the receptors.

Table A.2. Table of the initial conditions (nM) for each species.

TCR	10.0
pTCR	0.0
CTLA4	0.1
iTCR	0.0
CN	10.0
aCN	0.0
RCAN	0.1
aCN_RCAN	0.0
pRCAN	0.0
aCN_pRCAN	0.0
Carabin	0.1
aCN_Carabin	0.0
pNFAT	9.906
NFAT	0.001283
pNFAT_aCN	0.0
pNFAT_aCN_pRCAN	0.0
GSK3	4.507
NFAT_GSK3	0.0
mNFAT	0.1
mRCAN	0.1
pTAK1	0.0
RCAN_pTAK1	0.0
mCarabin	0.1
mTNFa	0.1
TNFa	0.12
TAK1	9.239
mCTLA4	0.1
mIL2	0.1
mFasL	0.1
IL2	0.1
FasL	0.1
Ras	10.0
aRas	0.0
aRas_Carabin	0.0
MEK	10.0
aRas_MEK	0.0
pMEK	0.0
Rac1GTP	0.1078
Rac1GTP_MEK	0.0
ERK	10.0

pMEK_ERK	0.0
pERK	0.0
PI3K	10.0
pIL2R	9.442
PI3K_pIL2R	0.0
PI3K_pTCR	0.0
aPI3K	0.0
PP2A	10.0
PP2A_CTLA4	0.0
aPP2A	0.0
Akt	8.853
Akt_aPI3K	0.0
pAkt	1.147
pAkt_aPP2A	0
GSK3_pAkt	0.0
pGSK3	5.493
Rac1GDP	9.892
Rac1GDP_aPI3K	0.0
IL2R	0.5258
IL2R_IL2	0.0
iIL2R	0.03187
mCISH	0.1
CISH	10.0
mPLCg	0.1
PLCg	10.0
PLCg_pTCR	0.0
pPLCg	0.0
pPLCg_CISH	0.0
PLCg_CISH	0.0
uPLCg	0.0
mPD1	0.1
PD1	0.1
aRas_PD1	0.0
aPI3K_PD1	0.0
E1	1.0

Table A.3. Upper and lower bounds of model parameters.

Parameter Type	**Lower Limit**	**Upper Limit**	**Units**	**Reference**	**Description**
kon	10^{-3}	1.0	$nM^{-1}min^{-1}$	Assumed	Association rate
KD_i	1.0	10^6	nM	Assumed	Binding affinity
kc_i	0.0	$6*10^4$	min^{-1}	[93]	Catalytic rate in Michaelis-Menten equations
kp_i	0.0	$6*10^4$	min^{-1}	[93]	Catalytic rate
v_i (for catalytic reaction)	10^{-4}	10^5	$nM*min^{-1}$	[5], [93]	Maximum velocity in Michaelis-Menten equations for unknown enzyme
v_i (for expression rate based on mRNA concentration)	10^{-4}	10^3	$nM*min^{-1}$	Assumed	Maximum velocity in Michaelis-Menten equations for protein production based on mRNA expression
km_i	10.0	10^5	nM	[5], [8]	Michaelis-Menten constant
$kgen_i$	10^{-6}	0.4	$nM*min^{-1}$	Estimated based on [1], [2], [3], [4]	Baseline generation rate of mRNAs
$kdeg_i$ (mRNA)	0.008	0.23	min^{-1}	[94]	Baseline degradation rate of mRNAs
$kdeg_i$ (proteins)	0.00008	0.0012	min^{-1}	[95]	Baseline degradation

					rate of proteins

Table A.4. Fitted parameters.

Parameter	**Values**	**Units**
kon	0.744759	$nM^{-1}min^{-1}$
KD4	223700.1	nM
KD5	168118.4	nM
KD6	45002.22	nM
KD7	35960.29	nM
KD8	78363.78	nM
KD9	722630.7	nM
KD10	415214.8	nM
KD13	453032.9	nM
KD14	961656	nM
KD15	293.516	nM
KD16	906154.5	nM
KD17	170870.2	nM
KD18	677861.2	nM
KD19	20799.91	nM
KD20	451422.9	nM
KD21	109834.2	nM
KD22	243654.7	nM
KD23	981692.4	nM
KD24	9437.089	nM
KD25	779131.4	nM
KD26	247916.6	nM
KD28	142418.6	nM
KD29	426916.3	nM
kp2	52917.64	min^{-1}
kp3	47468.17	min^{-1}

kp4	17341.5	min^{-1}
kp5	46471.26	min^{-1}
kp8	53.5484	min^{-1}
kp9	58494.47	min^{-1}
kp10	22373.75	min^{-1}
kp11	37764.75	min^{-1}
kp12	14643.93	min^{-1}
kp13	47265.41	min^{-1}
kp14	29050.98	min^{-1}
kp15	45695.24	min^{-1}
kp16	49236.73	min^{-1}
kp17	130.4833	min^{-1}
kp18	59510.23	min^{-1}
kp19	28986.8	min^{-1}
kp20	15644.21	min^{-1}
kp22	53384.22	min^{-1}
kp23	15354.08	min^{-1}
kc5a	57388.77	min^{-1}
kc1	26783.54	min^{-1}
kc2	25227.83	min^{-1}
kc37	10702.25	min^{-1}
kc38	45070.62	min^{-1}
kc39	59.07676	min^{-1}
v6a	1940.749	$nM*min^{-1}$
v3	42764.89	$nM*min^{-1}$
v4	67904.71	$nM*min^{-1}$
v5	16506.41	$nM*min^{-1}$
v6	764.9546	$nM*min^{-1}$
v7	841.3915	$nM*min^{-1}$
v8	51.22405	$nM*min^{-1}$
v9	243.4736	$nM*min^{-1}$
v10	71250.36	$nM*min^{-1}$
v11	951.8989	$nM*min^{-1}$
v12	994.5142	$nM*min^{-1}$
v13	887.4255	$nM*min^{-1}$
v14	322.8619	$nM*min^{-1}$
v15	64820.01	$nM*min^{-1}$
v16	921.2605	$nM*min^{-1}$
v17	367.4828	$nM*min^{-1}$
v18a	66755.12	$nM*min^{-1}$
v18b	90244.25	$nM*min^{-1}$
v19	95.03896	$nM*min^{-1}$
v20a	99478.15	$nM*min^{-1}$

v20b	66403.2	$nM*min^{-1}$
v21	754.1809	$nM*min^{-1}$
v22	93567.16	$nM*min^{-1}$
v23	73934.94	$nM*min^{-1}$
v24	30499.61	$nM*min^{-1}$
v25	17172.81	$nM*min^{-1}$
v26	11686.16	$nM*min^{-1}$
v27	29234.4	$nM*min^{-1}$
v28	57883.74	$nM*min^{-1}$
v29	30073.09	$nM*min^{-1}$
v30	75811.64	$nM*min^{-1}$
v31	92779.58	$nM*min^{-1}$
v32	0.135135	$nM*min^{-1}$
v33	999.735	$nM*min^{-1}$
v34	69.27322	$nM*min^{-1}$
v35	941.9566	$nM*min^{-1}$
v36	441.9933	$nM*min^{-1}$
km6a	91278.7	nM
km5a	22127.18	nM
km1	54590.13	nM
km2	58320.07	nM
km3	72420.89	nM
km4	29245.67	nM
km5	98188.35	nM
km6	4236.314	nM
km7	26841.6	nM
km8	38745.78	nM
km9	46150.41	nM
km10	77655.69	nM
km11	6575.344	nM
km12	5268.861	nM
km13	23090.31	nM
km14	69872.06	nM
km15	42230.83	nM
km16	7757.289	nM
km17	81674.67	nM
km18	44431.25	nM
km18b	22899.24	nM
km19	74325.13	nM
km20	7061.907	nM
km20b	62219.96	nM
km21	12292.1	nM
km22	887.574	nM

km23	50621.05	nM
km24	65056.24	nM
km25	89176.11	nM
km26	95710.72	nM
km27	99814.19	nM
km28	39089.5	nM
km29	71266.83	nM
km30	37001.62	nM
km31	9628.729	nM
km32	99987.58	nM
km33	2930.999	nM
km34	67837.13	nM
km35	24243.93	nM
km36	62854.4	nM
km37	64706.31	nM
km38	61341.04	nM
km39	99669.55	nM
kgen1	0.09331	$nM*min^{-1}$
kgen2	0.123895	$nM*min^{-1}$
kgen3	0.010411	$nM*min^{-1}$
kgen4	0.234104	$nM*min^{-1}$
kgen5	0.120324	$nM*min^{-1}$
kgen6	0.081743	$nM*min^{-1}$
kgen7	0.121839	$nM*min^{-1}$
kgen8	0.399069	$nM*min^{-1}$
kgen9	0.373886	$nM*min^{-1}$
kdeg1	0.054886	min^{-1}
kdeg2	0.000438	min^{-1}
kdeg3	9.35E-05	min^{-1}
kdeg4	0.190494	min^{-1}
kdeg5	0.000476	min^{-1}
kdeg6	0.009132	min^{-1}
kdeg7	8.59E-05	min^{-1}
kdeg8	0.110141	min^{-1}
kdeg9	9.63E-05	min^{-1}
kdeg10	0.15187	min^{-1}
kdeg11	0.001123	min^{-1}
kdeg12	0.229291	min^{-1}
kdeg13	0.000541	min^{-1}
kdeg14	0.149548	min^{-1}
kdeg15	0.000816	min^{-1}
kdeg16	0.11542	min^{-1}
kdeg17	0.001096	min^{-1}

kdeg18	0.227438	min^{-1}
kdeg19	0.000107	min^{-1}
kdeg20	0.000353	min^{-1}
kdeg21	0.021341	min^{-1}
kdeg22	8.27E-05	min^{-1}
log10_sigma1	-0.47502	
log10_scale1	-0.18046	
log10_offset1	0.18815	
log10_sigma2	-2.25911	
log10_scale2	-2.29188	
log10_offset2	-4.37036	
log10_sigma3	-1.63241	
log10_scale3	-1.36121	
log10_offset3	-0.25962	
log10_sigma4	-2.3683	
log10_scale4	0.373133	
log10_offset4	-4.99998	
log10_sigma5	-0.88629	
log10_scale5	1.055226	
log10_offset5	0.062407	
log10_sigma6	-0.77074	
log10_scale6	1.490558	
log10_offset6	-0.13829	
log10_sigma7	1.341567	
log10_scale7	-1.00375	
log10_offset7	1.494577	
log10_sigma8	2.227199	
log10_scale8	0.940156	
log10_offset8	-4.98264	
log10_sigma9	-2.9999	
log10_scale9	-3.62915	
log10_offset9	-4.69992	
log10_sigma10	1.294673	
log10_scale10	0.684183	
log10_offset10	2.120215	
log10_sigma11	-0.77374	
log10_scale11	-2.5305	
log10_offset11	-0.76581	
log10_sigma12	1.049281	
log10_scale12	-1.54426	
log10_offset12	1.226346	
log10_sigma13	-2.9999	
log10_scale13	-0.98793	

log10_offset13	-0.05328	

References

[1] B. Jones, D. Stekel, J. Rowe, and C. Fernando, "Is there a liquid state machine in the bacterium Escherichia coli?," *Proceedings of the 2007 IEEE Symposium on Artificial Life, CI-ALife 2007*, pp. 187–191, 2007, doi: 10.1109/ALIFE.2007.367795.

[2] H. Chen, K. Shiroguchi, H. Ge, and X. S. Xie, "Genome-wide study of mRNA degradation and transcript elongation in Escherichia coli," *Mol Syst Biol*, vol. 11, no. 1, p. 781, Jan. 2015, doi: 10.15252/MSB.20145794.

[3] S. Kühner *et al.*, "Proteome organization in a genome-reduced bacterium," *Science (1979)*, vol. 326, no. 5957, pp. 1235–1240, Nov. 2009, doi: 10.1126/SCIENCE.1176343.

[4] J.-M. Anaya, Y. Shoenfeld, A. Rojas-Villarraga, R. A. Levy, and R. Cervera, "Autoimmunity," *Autoimmunity: From Bench to Bedside*, pp. 237–378, Jul. 2013, Accessed: Jun. 11, 2025. [Online]. Available: https://www.ncbi.nlm.nih.gov/books/NBK459447/

[5] D. Davidia *et al.*, "Global characterization of in vivo enzyme catalytic rates and their correspondence to in vitro kcat measurements," *Proc Natl Acad Sci U S A*, vol. 113, no. 12, pp. 3401–3406, Mar. 2016, doi: 10.1073/PNAS.1514240113.

[6] Y. Wang, C. L. Liu, J. D. Storey, R. J. Tibshirani, D. Herschlag, and P. O. Brown, "Precision and functional specificity in mRNA decay," *Proc Natl Acad Sci U S A*, vol. 99, no. 9, pp. 5860–5865, Apr. 2002, doi: 10.1073/PNAS.092538799,.

[7] S. B. Cambridge, F. Gnad, C. Nguyen, J. L. Bermejo, M. Krüger, and M. Mann, "Systems-wide proteomic analysis in mammalian cells reveals conserved, functional protein turnover," *J Proteome Res*, vol. 10, no. 12, pp. 5275–5284, Dec. 2011, doi: 10.1021/PR101183K.

[8] S. Y. Shin, M. W. Kim, K. H. Cho, and L. K. Nguyen, "Coupled feedback regulation of nuclear factor of activated T-cells (NFAT) modulates activation-induced cell death of T cells," *Sci Rep*, vol. 9, no. 1, p. 10637, Dec. 2019, doi: 10.1038/S41598-019-46592-Z.